IOP Publishing Journal of Physics D: Applied Physics

J. Phys. D: Appl. Phys. **47** (2014) 383001 (23pp) doi:10.1088/0022-3727/47/38/383001

Topical Review

Controlling strongly correlated dust clusters with lasers

Hauke Thomsen[1], **Patrick Ludwig**[1], **Michael Bonitz**[1,4], **Jan Schablinski**[2], **Dietmar Block**[2], **André Schella**[3] and **André Melzer**[3]

[1] Institut für Theoretische Physik und Astrophysik, Christian-Albrechts-Universität zu Kiel, 24098 Kiel, Germany
[2] Institut für Experimentelle und Angewandte Physik, Chrsitian-Albrechts-Universität zu Kiel, 24098 Kiel, Germany
[3] Institut für Physik, Ernst-Moritz-Arndt-Universität Greifswald, 17487 Greifswald, Germany

E-mail: thomsen@theo-physik.uni-kiel.de, ludwig@theo-physik.uni-kiel.de, bonitz@physik.uni-kiel.de, schablinski@physik.uni-kiel.de, block@physik.uni-kiel.de, schella@physik.uni-greifswald.de and melzer@physik.uni-greifswald.de

Received 4 March 2014, revised 2 June 2014
Accepted for publication 1 July 2014
Published 28 August 2014

Abstract

Lasers have been used extensively to manipulate matter in a controlled way – from single atoms and molecules up to macroscopic materials. They are particularly valuable for the analysis and control of mesoscopic systems such as few-particle clusters. Here we report on recent work on finite size complex (dusty) plasma systems. These are unusual types of clusters with a very strong inter-particle interaction so that, at room temperature, they are practically in their ground state. Lasers are employed as a tool to achieve excited states and phase transitions.

The most attractive feature of dusty plasmas is that they allow for a precise diagnostic with single-particle resolution. From such measurements, the structural properties of finite two-dimensional (2D) clusters and three-dimensional (3D) spherical crystals in nearly harmonic traps—so-called Yukawa balls—have been explored in great detail. Their structural features—the shell compositions and the order within the shells—have been investigated and good agreement to theoretical predictions was found. Open questions on the agenda are the excitation behaviour, the structural changes and phase transitions that occur at elevated temperature.

Here we report on recent experimental results where laser heating methods were further improved and applied to finite 2D and 3D dust clusters. Comparing to simulations, we demonstrate that laser heating indeed allows to increase the temperature in a controlled manner. For the analysis of thermodynamic properties and phase transitions in these finite systems, we present theoretical and experimental results on the basis of the instantaneous normal modes, pair distribution function and the recently introduced centre-two-particle correlation function.

Keywords: dusty plasmas, laser heating, phase transitions, strong correlations

(Some figures may appear in colour only in the online journal)

1. Introduction

Complex (dusty) plasmas differ from traditional plasmas in a number of aspects: complex plasmas, in very general terms, are multicomponent plasmas that contain, in addition to electrons, ions and neutral atoms, also (macro-)molecules.

This may lead to substantial chemical reactivity or growth of clusters or nanoparticles that are of high interest for technological applications, see e.g. [1–4]. Alternatively, macroscopically large particles (dust) can be introduced into the plasma externally which may radically alter the plasma properties. These 'dusty plasmas' have evolved into a separate research field and are the subject of this review. Here, we

---

[4] Author to whom any correspondence should be addressed.

focus on non-reactive dusty plasmas containing comparatively large—typically micrometer sized—monodisperse plastic spheres.

The unusual properties of these plasmas arise from the behaviour of the dust particles and their enormously high charge. In the plasma, the particles are subject to continuous bombardment by the much lighter electrons, ions and neutrals. In a radio frequency (rf) discharge, the electron temperature is way above the ion temperature resulting in a higher impact rate of electrons onto the originally neutral particles, compared to the ions. As a consequence the particles become highly negatively charged, with the charge reaching values on the order of $Q_\mathrm{d} = \mathcal{O}(-10\,000\,e)$ elementary charges for a particle of micron size [5]. It is due to this high negative charge that the dust particles are strongly interacting with each other, and the dust component of the plasma aquires a very large electrostatic energy that may exceed the thermal energy by orders of magnitude: the dust becomes *strongly coupled* (or strongly correlated), in striking contrast to usual high-temperature plasmas. At the same time electrons and ions are only weakly coupled and can often be regarded as a more or less uniform background.

Such strong correlation effects are presently of high interest in a large variety of fields, including condensed matter, dense plasmas (such as warm dense matter), ultracold quantum gases or the quark-gluon plasma. In fact, dusty plasmas serve as a prototype for studying correlation phenomena, e.g. [6]. A particular advantage of dusty plasmas is the large particle size and large inter-particle spacing (on the order of several micrometers to millimeters) which allows for a direct optical imaging of individual particles. At the same time the large mass results in slow characteristic time scales (on the order of hundreds of milliseconds), so the whole dynamics of these plasmas can be studied on the single-particle 'atomic' level [1, 3]. Despite the purely classical behaviour, dusty plasmas allow for unique and unprecedentedly accurate diagnostics of strong correlation effects which are important for other strongly correlated systems where such diagnostics are missing.

To have a quantitative measure of correlation effects in these highly non-ideal charged particle systems, it has been common to use the Coulomb coupling parameter Γ that relates the mean Coulomb interaction energy of two particles to the thermal energy as[5]

$$\Gamma = \frac{Q_\mathrm{d}^2}{4\pi\varepsilon_0\, b_\mathrm{WS}} \frac{1}{k_\mathrm{B} T_\mathrm{d}}, \tag{1}$$

where the Coulomb interaction is estimated by the one of two particles separated by the Wigner–Seitz radius, that is related to the density by $n^{-1} = 4\pi b_\mathrm{WS}^3/3$ in three-dimensional (3D) ($n^{-1} = \pi b_\mathrm{WS}^2$ in two-dimensional (2D)[6]), and T_d is the kinetic temperature that corresponds to the dust particles' random motion. In ideal (or weakly non-ideal), conventional plasmas $\Gamma \ll 1$. If Γ exceeds unity, the system is strongly coupled and the particle arrangement exhibits an increasingly long range order, giving rise to liquid-like behaviour. If Γ exceeds about one hundred the interaction is strong enough to spatially localize the particles leading to a crystalline structure. In macroscopic Coulomb systems, the critical value for the freezing transition is around $\Gamma = 175$ in 3D and $\Gamma = 137$ in 2D [8–10].

Extended (nearly macroscopic) dust systems in 2D and 3D have been realized in experiments for decades, see e.g. [11–16]. There, Γ values of several hundreds are easily achieved, even at room temperature, as will be discussed in sections 5.2 and 6. At these conditions the system is practically in its ground state. Therefore—and this may be surprising—for dusty plasmas, the major challenge for many applications is to *lower the coupling strength*. The main task is to do this in a controlled manner for instance by increasing only the dust temperature T_d, without affecting the other plasma parameters. This is particularly important in order to study the thermodynamic properties, the melting process and the different phases of these systems. To achieve a controlled heating of dust clusters several methods have been used, including variation of the rf power or the neutral gas pressure [17–20]. However, these methods usually alter the whole discharge environment and, thus, effectively create a different plasma, making a 'clean' analysis of dust thermal effects difficult [17, 21].

1.1. Laser heating of dust in the context of laser–matter interaction

A suitable approach to heat the dust without affecting the discharge environment is the use of lasers which is, therefore, in the focus of the present review. Since laser manipulation has become common in many fields it is of interest to put the present activities in the field of dusty plasmas into a broader perspective, before moving on.

The control of matter by lasers has seen dramatic progress over the last two decades which is due to the rapid increase of available coherent radiation sources. These are, in first place, optical and infrared lasers but, with the progress in the field of harmonic generation as well as of free electron lasers, also high photon energies—from UV to soft x-rays—became available. At the same time a tremendous variety of methods and mechanisms to control matter with lasers is being utilized which is briefly summarized in table 1. There we list the main properties of coherent electromagnetic radiation and how they are applied in different areas.

Traditionally, lasers have been used to excite electronic transitions in atoms and molecules allowing for high precision spectroscopy. By choosing a particular laser polarization, certain transitions can be activated or deactivated depending on the selection rules. In case of laser excitation of electrons into the continuum (photoionization) the photoelectron spectrum reveals detailed information on the target material. Related methods such as photoelectron spectroscopy are highly successful in atomic, molecular and condensed matter physics.

---

[5] Strictly, the definition (1) is an appropriate measure for the potential energy only when the pair interaction is Coulombic. In the case of screening, the effective coupling parameter depends on the screening length λ_D [7]. For the results reported in this paper, the dustâŁ"dust interaction is moderately screened and the definition (1) is sufficiently accurate.

[6] For macroscopic systems, the Coulomb coupling parameter is clearly defined by the condition that each particle occupies, on average a spherical volume (a circle in 2D) with the radius equal to b_WS.

Table 1. Examples of laser–matter interaction processes in macroscopic systems (for details and references see main text). The concepts presently being used in dusty plasmas are highlighted in bold, see also table 2. Note that in many applications several laser properties are active simultaneously and the highlighted property should only be understood as the dominant one.

Laser property	Applications and mechanisms
photon energy $N\hbar\omega, \quad N = 1, 2, \ldots$	• (multi-)photon excitation and ionization of atoms, molecules, condensed matter etc. • photoemission spectroscopy • inverse bremsstrahlung heating of matter • **photoionization of dust particles**
laser polarization	• selection of intra-atomic (intra-molecular) transitions, e.g. linear vs. circular polarization
electrical field strength E, potential energy $-eEx$	• tunnel and field ionization of atoms • field assisted creation of electron-positron pairs (Schwinger mechanism)
laser intensity, $I \sim E^2$ Ohmic heat	• heating, melting, evaporation of matter • ionization of matter, creation of dense plasmas
light pressure, $p \sim I$	• structuring of surfaces, micro-hole boring • **acceleration of single dust particles**
short pulse duration	• time-resolved diagnostics (e.g. pump-probe schemes) • rapid excitation of non-equilibrium phenomena • non-thermal melting of solids
field gradient of standing wave	• **charge confinement, 'optical tweezers'** • confinement of neutral particles in optical lattices
field gradient of moving wave	• charged particle trapping • laser wake field acceleration

With the increase of laser intensity also nonlinear processes such as multi-photon excitation and ionization have become available. In complex plasmas containing reactive species spectroscopic methods have found broad application as well, e.g. [2, 3] and references therein, but this has not been relevant for dusty plasmas so far. At the same time, ionization by UV radiation has been discussed by some groups [22–26], but has proven to be difficult. The interesting prediction is that the dust particles acquire a positive charge, but this will not be considered in the present paper.

Another important concept is the use of laser radiation with a spatially inhomogeneous intensity profile such as focused beams or interference patterns of several lasers. The latter gives rise to optical traps or optical lattices and has become a key tool in the field of ultracold atoms and molecules, e.g. [27] or in the field of colloidal systems, where laser patterns have been used to create quasi-crystals [28, 29]. Furthermore, the spatially varying field of a moving laser wave is at the heart of particle acceleration predicted long ago [30, 31]. In the mean time laser wake field acceleration has been successfully realized experimentally and allows for the generation of relativistic electron beams with MeV energy [32–36] as well as for ion acceleration. In dusty plasmas laser beams with spatially varying intensity profile are exploited utilizing the intensity dependence of the index of refraction of dust particles allowing to trap and move single particles ('laser tweezers') [37–39], see also [40].

An alternative direction in laser–matter interaction is heating of matter by generating Ohmic heat. Acceleration of electrons in solids easily allows to couple laser energy into the material and to melt it. This has become a standard method in technology and is used e.g. for microsopic structuring of surfaces as well as for drilling high quality micrometer-size holes. With the availability of ultrashort laser pulses it has become possible to couple the energy in a controlled way only into the electron subsystem, without heating the lattice, and to probe—on a femtosecond time scale—the 'non-thermal melting' of solids far from equilibrium, e.g. [41, 42]. Lasers can also be directly used to heat plasmas, via photon absorption in electron–ion collisions (inverse bremsstrahlung), e.g. [43–45] and references therein. With the help of Petawatt lasers, the combination of laser ionization and particle acceleration allows to produce and compress plasmas which reach densities that are comparable to and even exceed by one or two orders that of metals. This has led to the new fields of laser plasmas or high energy density physics, e.g. [46, 47]. It has been predicted long ago that sufficiently high laser intensities will allow to achieve even fusion conditions [48].

The heating of dusty plasmas follows the same general idea of transmitting momentum and energy from the radiation to the particle ensemble by exploiting the light pressure but, obviously, using very modest laser intensities. The specifics here lie in the large particle size, compared to the typical laser focus, and in the peculiar properties of finite dust clusters. These mesoscopic particle ensembles have many properties in common with more traditional neutral or metal clusters and will be discussed below.

1.2. Finite dust clusters and comparison with metal clusters

The properties of finite systems have been first studied in nuclear matter and more recently in the context of cluster physics. Finite 2D and spherical 3D dust clusters in a (nearly) isotropic harmonic trap provide a fascinating opportunity

Table 2. Comparison of atomic clusters (example of metal clusters) with finite dust clusters. In the lower part the relevant cluster manipulation approaches by means of lasers are outlined. Comments: a–streaming electrons and ions may give rise to anisotropic and even attractive dust–dust interaction, depending on the plasma parameters and location in the discharge, e.g. [63–65].

Property	Metal clusters	Dust clusters
size, geometry	$N \sim 10 \ldots 10^4$; 3D	$N \sim 10 \ldots 10^4$; 2D, 3D
elementary constituents	single atoms	spherical plastic particles
particle radius R	$R \sim a_B$	$R \sim 1 \ldots 10\,\mu$m
interparticle distance $\bar{r}$	$\bar{r} \sim$ few a_B	$\bar{r}$ several 100 μm
confinement	attraction from central ionic core	external potentials: trap, thermophoresis etc.
pair interaction	Coulomb repulsion between electrons	screened Coulomb (Yukawa) repulsion
interaction strength	fixed	externally controlled
coupling parameter	valence electrons: $r_s = \bar{r}/a_B \sim 2 \ldots 5$	dust component: $\Gamma = E_{\mathrm{int}}/E_{\mathrm{kin}} \sim 10 \ldots 10^4$
stationary state	equilibrium	non-equilibrium^a
ground state	concentric shells	concentric shells
Laser manipulation	$\sigma \gg R, \bar{r}$	$\bar{r} \gtrsim \sigma > R$
laser spot size σ	homogeneous field across cluster	fast spot movement: on average homogeneous force across cluster
	• photoionization, • collective ionization • Coulomb explosion	• single-particle diagnostics by light scattering • particle control by optical tweezers
laser heating	• via inv. bremsstrahlung	• via light pressure

to systematically study the physics of mesoscopic few-particle systems. The reason is the above mentioned unique opportunity provided by dusty plasmas to study structure, dynamics and thermodynamics of *all* individual system particles on the kinetic level, i.e. resolving simultaneously all particle trajectories. This is of high interest for finite systems in a variety of other fields including gas or metal clusters, electrons in quantum dots, trapped ions, ultracold gases and so on. In none of these fields observations on the kinetic level are possible.

Finite 2D clusters have been studied first, already for quite some time [49–54]. More recently also spherical 3D dust crystals could be produced [55], and their low-temperature structure (which, in general, is more sensitive to screening than for 2D systems) is now well understood (for details see section 2.2). In the case of strong coupling, the excitation behaviour is dominated by collective modes of the whole system rather than by single particle dynamics. This is typical not only for finite dust clusters but for mesoscopic systems in trapping potentials in general. The frequency of some of these normal modes (in particular that of the monopole or 'breathing' oscillation) has been found sensitive to the internal properties of finite systems such as type of interaction [56, 57, 59] and, in the case of quantum clusters, also on the interaction strength (on the coupling parameter) [58] or particle number [60]. This has led to the idea to use the normal mode frequencies as a novel kind of 'spectroscopy' for strongly correlated finite systems [61], for a recent overview see [62].

Of particular interest is the gradual crossover, with increased cluster size [49, 53], from single atoms to macroscopic condensed matter [66, 67]. In this field, also the interaction of lasers with finite clusters has been studied in great detail. Due to the similarity of these systems to the finite dust clusters that are in the focus of this review we provide some comparison in table 2. In both cases clusters in a similar range of particle number are studied. The main difference is the different type of particles—atoms (or molecules) versus highly charged plastic spheres—and the different type of confinement. In the case of metal clusters the valence electrons are kept together by the central Coulomb force from the ionic core of the cluster. In contrast, in the case of dust clusters the pair interactions are purely repulsive and the confinement is provided by an external potential (or combinations thereof). Another key difference is that, in metal clusters, the coupling strength is fixed by the governing Coulomb forces between all particles. In contrast, in dust clusters the charge of the grains and their distance can be modified by changing the plasma parameters. Nevertheless, the dust systems usually feature only relatively large values of the coupling parameter Γ.

Among the most interesting questions both for finite metal clusters and finite dust clusters is the size dependence of their properties. This includes the ground state structure, the excitation spectrum and the thermodynamic properties. Since a central topic of this review is phase transitions this involves the question of size dependent melting temperatures. It is known for a long time that the melting temperature of small clusters is lower than the bulk melting temperature. This topic has been studied for metal clusters in some detail. We mention experimental studies, e.g. [68–70] and references therein, theoretical work, e.g. [71, 72] as well as computer simulations, e.g. [73, 74]. There is overall consensus that the melting temperature of such clusters with short-range interaction decreases proportional with the cluster diameter. For harmonically confined Coulomb clusters [75] also a decrease of the melting temperature was observed in simulations which is almost linear in the fraction of particles in the surface layer. For dust clusters, no such general trend is known yet due to the lack of systematic studies of larger clusters and due to the difficulties in controlled cluster heating. The laser heating technique described in this review will pave the way towards such studies.

When lasers where first shot on finite metal clusters, the experiments revealed a surprisingly effective energy absorption [76]. Subsequently, also collective absorption mechanisms (by coupling to plasmons) were observed [77, 78]. These effects could be successfully explained by theoretical modelling [79] and complex many-particle simulations, for an overview see [80]. Among the theoretical difficulties is the proper treatment of electronic quantum many-body effects, see e.g. [81, 82]. A detailed discussion of the various laser–cluster interaction mechanisms has been given in [83], see also the recent reviews [80, 84].

Among the most interesting effects of laser illumination of metal clusters is the emission of higher harmonics of the laser radiation [85], the emission of energetic electrons and, in case of strong ionization, Coulomb explosion of the whole cluster [86]. A similar rapid expansion of Coulomb and Yukawa dust clusters has been recently predicted in [87]. Here laser illumination is not necessary at all, it is sufficient to turn off the confinement potential. Similarly, many other effects observed for metal clusters in the presence of intense laser radiation can also be expected for dust clusters. However, more recently the focus was on a gentle heating of dust clusters so that the system is transfered from its ground state into a state with moderately elevated temperature.

As discussed above a focused low intensity laser beam is well capable to accelerate single dust particles. Similarly, stationary laser beams were used to excite shear flows in monolayer dust crystals [88, 89] or rotations in finite 2D clusters [53]. Mach cones could be excited by moving the laser spot through the dust crystal [90, 91]. A further application of moving laser spots is the realization of a heat source for the dust component [92–95]. A more detailed description of these pioneering laser experiments is given in section 3.1. An improved heating scheme allowing to realize a true thermodynamic heating with an isotropic, Maxwellian 2D velocity distribution has been applied by Schablinski *et al* [96] to finite 2D dust clusters. A first heating concept for finite 3D clusters has been realized by Schella *et al* [97], see section 5.2.

The goal of this review article is to present an overview on these recent experimental developments, compare them to theory and computer simulations and to discuss possible future applications of laser manipulation of dust clusters. We start by giving a brief overview on the properties of finite 2D and 3D dust clusters in section 2. Then, we discuss the laser heating principle and how it is used to reduce the coupling strength in a controlled way (section 3). Dedicated numerical simulations of the laser heating are presented in section 4. Experimental results for finite 2D and 3D dust systems are presented in sections 5.2 and 6. We conclude in section 7 with an outline of future applications, including spatially inhomogeneous plasmas and time-dependent processes.

2. Structural, thermodynamic and transport properties of finite dust clusters

2.1. Structural properties of extended dust clusters

As described in the introduction, electrons and ions screen the repulsive interaction of the dust grains. The interaction between the dust particles is, in most cases, well described by a Yukawa-type pair-potential

$$\Phi_\mathrm{Y}\left(\vec{r}_i,\vec{r}_j\right)=\frac{Q_\mathrm{d}^2}{4\pi\varepsilon_0\left|\vec{r}_i-\vec{r}_j\right|}\cdot\mathrm{e}^{-\kappa\left|\vec{r}_i-\vec{r}_j\right|},\tag{2}$$

where $\kappa=\lambda_\mathrm{D}^{-1}$ is given by the inverse Debye length taking into account the screening effect of electrons and ions[7]. Wake effects due to the streaming ions (for recent overviews see e.g. [63–65]) are neglected in the presented results.

Extended 2D dust systems arrange, in the solid state, in a hexagonal lattice [11–13]. These systems are of special interest since the mechanism of thermodynamic phase transition in 2D systems from the ordered solid phase to the unordered liquid phase is still not finally clarified [98]. On the one hand, a first-order transition is predicted by the formation of grain boundaries between crystalline patches [98, 99]. On the other hand, a two-step second-order transition with an intermediate hexatic phase, the so-called KTHNY scenario [98, 100–102], is expected. A recent numerical study concludes that the hexatic phase is metastable and vanishes in the long-time limit [103]. Thermodynamic heating of 2D dust crystals by means of laser techniques might, therefore, be very beneficial in addressing these issues from the experimental side, see section 5.1.

2.2. Structural properties of finite dust clusters

The striking property of solid Yukawa clusters in 2D as well as in 3D is their well ordered structure. This structure and the loss of order with increasing temperature is accompanied by a sequence of phase transitions (or structural transitions) which are peculiar in finite systems [51, 104]. Details of these transitions are still open and of high interest for many finite size systems. They depend on the particular crystal structure which we, therefore, review in the following.

The Hamiltonian of the N-particle Yukawa cluster is (prior to laser manipulation) given by [3]

$$\mathcal{H}=\sum_{i=1}^{N}\frac{1}{2m}\vec{p}_i^{\,2}+\sum_{i=1}^{N}\frac{m\omega_0^2}{2}\vec{r}_i^{\,2}+\sum_{i<j}\Phi_\mathrm{Y}\left(\vec{r}_i,\vec{r}_j\right),\tag{3}$$

where the first term describes the kinetic energy, the second the confinement energy due to the harmonic trap of strength ω_0 and the third the mutual Yukawa interaction energy. In this model, all dust grains are assumed to be equal in mass m and charge Q_d.

Small 2D dust clusters typically consist of concentric rings [49, 51]. The core region of larger clusters with several

---

[7] The Debye length $\lambda_\mathrm{D}=\left(\frac{q_\mathrm{e}^2\bar{n}_\mathrm{e}}{\varepsilon_0k_\mathrm{B}T_\mathrm{e}}+\frac{q_\mathrm{i}^2\bar{n}_\mathrm{i}}{\varepsilon_0k_\mathrm{B}T_\mathrm{i}}\right)^{-1/2}$ incorporates screening of electrons and ions. q_e (q_i) is the electron (ion) charge, $\bar{n}_e$ ($\bar{n}_i$) is the average electron (ion) density and T_e (T_i) is the electron (ion) temperature.

hundred particles, in contrast, shows a hexagonal structure, like in infinite systems. This lattice has dislocations at the outer shells, where the circular boundary has to be matched [105].

Finite 3D dust clusters consist of spherical shells instead of rings [55, 106]. Due to their spherical shape, these clusters are called *Yukawa balls* (or *Coulomb balls*, when screening can be neglected). This structure has been measured experimentally [55, 107] and is reproduced in first-principle simulations–molecular dynamics (MD) or Monte Carlo (MC)–and has been investigated in detail for both Coulomb balls [108–110] and Yukawa balls [111, 112]. The general trend is that, when the screening parameter κ increases, more particles occupy the inner shells, and—even in the ground state—the average density becomes inhomogeneous, decaying towards the cluster boundary [113, 114]. This is in striking contrast to classical Coulomb clusters which have, at $T = 0$, a homogeneous mean density[8].

Recently, also several analytical theories for the shell structure in 3D have been developed. The *local density approximation* as a continuum theory accurately describes the mean density profile of the spherical clusters [113, 114], but it misses the formation of shells. The positions and the populations of the shells of Coulomb balls are well reproduced by a slightly modified version of the *hypernetted chain approximation* which can be adapted to particles interacting via a Yukawa potential as well [115–118]. Beyond the radial shell structure, 3D dust balls exhibit a well ordered intra-shell structure at strong coupling. In contrast to a flat 2D system, the spherical curvature requires a fraction of pentagonal Voronoi cells in the hexagonal pattern on the shell [110, 119].

2.3. Thermodynamic properties and phase transitions

As the ground state properties of finite dust clusters are well understood by now [108–112], further investigations concentrate on thermodynamic properties at elevated temperatures. When a cluster is excited by feeding thermal energy into the system, metastable states with energies above the ground state energy $E_0(N, \kappa)$ are occupied. These metastable states may differ from the ground state with respect to the occupation numbers of the shells or in the particle configuration within the shells. The metastable states of Yukawa balls as well as their increased population with temperature were investigated in both experiment [107, 120] and first principle simulations [121, 122]. Among others, these simulations allowed to determine the heights of energy barriers between different metastable states [121–123]. This 'fine structure' [110] is observed for 3D but not for 2D clusters.

When the temperature is increased a transition from a well ordered structure with thin shells and a highly symmetric intra-shell order (3D) towards a disordered particle fluid-like state is observed. It is an interesting question whether this process occurs rapid and constitutes a phase transition, as in macrocscopic systems. While many similarities to phase transitions have indeed been observed[9], there are also differences: the first is that in finite systems 'melting' requires a finite temperature interval. The second is that melting may involve a sequence of distinct processes. Therefore, in order to resolve and understand these processes, the concepts for characterization of phase transitions known from macroscopic systems have to be re-considered and adapted. In particular, structural parameters are required that are suitable to characterize the phase transition. The first quantity that comes to mind is the heat capacity, (the amount of heat δQ required to heat up the system a temperature δT) which is a widely used melting parameter e.g. in solid state physics. However, measuring the heat capacity is challenging in dusty plasmas. The dust subsystem exchanges energy with electrons, ions and neutrals making it very difficult to extract the pure heat capacity of the dust system with a particle number that is negligible compared to the number of the surrounding plasma constituents [75]. In contrast, the pair distribution function and, even more, the C2P correlation, discussed in the next section, have proven to be well suited for this purpose in theory as well as in experiments.

Let us now summarize the known results about 'phase transitions' in finite dust systems. In two dimensions, for the loss of the ring structure, two different melting processes were identified. The first process is attributed to the rotation of one ring with respect to the other rings [51–53]. The required energy for such a rotation crucially depends on the exact occupation number of the rings. For example, the commensurate configuration ('magic number') $N = 19$ (1-6-12) is very stable against such inter-shell rotations (due to the matching particle numbers on the inner and outer shell this cluster has a perfect hexagonal symmetry). In contrast, the $N = 20$ (1-7-12) configuration is extremely unstable against this excitation [53] and has a drastically reduced inter-shell rotation barrier and melting temperature. The second melting process is associated with particles undergoing a transition between two adjacent rings and is called 'radial melting'. It, typically, takes place at substantially higher temperatures [21]. It is worth noting that the same kind of two-stage melting process is observed in finite quantum clusters [124, 125], indicating that these are correlation effects which are of high interest also beyond the field of dusty plasmas.

The complexity of the melting process increases when advancing from 2D to 3D clusters [123, 126]. Besides the melting of the radial structure and the inter-shell rotation, a third melting process emerges that is connected to the intra-shell order [126]. However, this classification is not strict since the interplay between the different melting processes in 3D clusters is utmost complex and there is, in general, no separation of the different processes. Thus many interesting questions are still open that have to be answered by experiments and theory.

In order to trigger phase transitions in dusty plasma experiments, selective control over the dust kinetic temperature

---

[8] Nevertheless, as a reasonable first approximation for the average density one can often use the particle number N and the radius of the outermost shell R_C, $\langle n\rangle \approx N/(4\pi R_C^3/3)$

[9] As the solid and fluid 'phases' are, strictly speaking, concepts defined in the macroscopic limit the same holds true with phase transitions. Nevertheless, the processes in many finite systems are very similar and the application of thermodynamic concepts is useful. Often though the term 'crossover' is preferred in comparison to phase transition.

is essential. In particular, it is desirable to feed energy into the random dust motion without changing other plasma parameters such as the neutral gas pressure, the electron and ion temperatures and the flow velocity of the ions. A further requirement is that the entire cluster should be heated homogeneously while preserving an isotropic velocity distribution. As will be described in detail in section 3, this selective control over the dust temperature is indeed possible—by the means of intense laser light.

2.4. Key quantities for the analysis of finite dust clusters

An important structural parameter that characterizes the order (and its loss during melting) in extended systems is the *radial pair distribution function* $g(r_{ij}) = g(|\vec{r}_i - \vec{r}_j|)$. It is commonly defined by the average number of particle pairs found at a distance of r_{ij} divided by the number of pairs which one would find in a homogeneous (i.e. uncorrelated) system with the same density. The first maximum of g reflects the mean inter-particle distance between the particles. An algebraic decay of the envelope of g over r_{ij} indicates a long range order, characteristic of the solid regime. Moreover, the height of the first maximum allows to detect a melting line in the (Γ, κ) space [7].

The radial pair distribution function for finite 2D and 3D clusters is shown in parts d of figures 2 and 3, respectively[10]. $g(r)$ drops to zero after a few nearest neighbour distances for finite clusters in both 2D and 3D. For obvious reason, a true 'long range behaviour' cannot be investigated for finite clusters. Nevertheless, $g(r)$ contains detailed information about the thermodynamic state of the cluster and its temperature dependence. In particular, a fine structure of the peaks in $g(r_{ij})$ is visible at high coupling strength (low temperature), indicating a frozen structure. When the temperature is increased, the subpeaks disappear. Finally, at a moderate coupling strength, see curve $\Gamma = 10$ in figure 2, the pair distribution function has only a single peak followed by a monotonous decay. The classification of inter-shell and intra-shell melting is not possible by means of this quantity as sampling the modulus of the distance does no distinguish whether the particles of a pair are on one shell or on different shells.

For this reason, the C2P correlation function $g_2(r_\mathrm{I}, r_\mathrm{II}, \varphi)$ is introduced which takes into account the radial position of both particles as well as their angular distance with respect to the trap centre [97, 127]. A sketch of the sampled coordinates is shown in figure 1 for a 3D Yukawa ball consisting of two spherical shells and one particle in the centre. To evaluate the C2P, the sampled two-particle probability density $\rho_2(r_\mathrm{I}, r_\mathrm{II}, \varphi)$ is computed and normalized by the uncorrelated probability density (i.e. the function which one would find in a system with the same radial structure but homogeneously filled shells) $\rho_2^{\mathrm{uncorr}}(r_\mathrm{I}, r_\mathrm{II}, \varphi)$,

$$g_2\left(r_\mathrm{I}, r_\mathrm{II}, \varphi\right) = \frac{\rho_2\left(r_\mathrm{I}, r_\mathrm{II}, \varphi\right)}{\rho_2^{\mathrm{uncorr}}\left(r_\mathrm{I}, r_\mathrm{II}, \varphi\right)}. \tag{4}$$

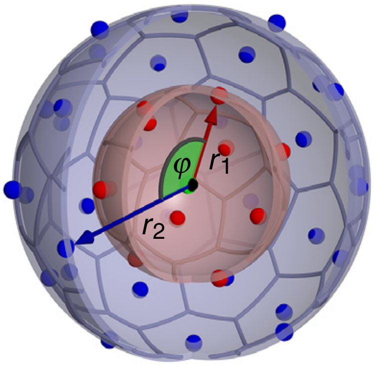

Figure 1. Yukawa ball with $N = 60$ particles consisting of two spherical shells and a single particle in the centre. In order to sample the centre-two-particle (C2P) correlation function based on the coordinates, for each particle pair, both radial coordinates r_I and r_II as well as the angular pair distance φ with respect to the trap centre are recorded. The Voronoi grid of the intra-shell particle configuration is shown in grey.

Since $\rho_2(r_\mathrm{I}, r_\mathrm{II}, \varphi)$ is invariant under rotation of the entire cluster, it is not necessary to remove a rigid rotation before sampling.

The C2P contains very detailed information on the structure of finite clusters and useful special cases. For example, integration of g_2 over both radial coordinates over a range corresponding to one shell allows one to extract the angular pair correlation function within that shell. On the other hand, when only one radius coordinate is integrated of the width of one shell, the C2P contains information on the relative radial and angular arrangement of the particles of the same shell as well as from different shells. To visualize this, $g_2(r_\mathrm{I}, \varphi)$ can be plotted in a color map, as is done for a 2D cluster, in figure 2, and a 3D cluster, see figure 3. In this color map, the intra-shell structure is responsible for the maxima and minima in φ-direction. While the data in the figures are from MC simulations, equally well one can use data from experiments with finite dust clusters, as is shown below in figure 12.

For the 2D cluster with $N = 25$ particles, depicted in figure 2, a reference particle from the inner shell is chosen by the integration range around $r_\mathrm{I} \approx 0.7$. Since the inner shell consists of three particles, the intra-shell neighbours appear as a peak at $\varphi = 120°$. At $\Gamma = 1000$, the distinct peaks found around $r_\mathrm{II} \approx 1.6$ show that the angular orientation of the second shell with nine particles is locked with respect to the inner shell. This inter-shell order disappears between $\Gamma = 1000$ and $\Gamma = 100$ where g_2 is smeared out in angular direction. At moderate coupling, $\Gamma = 10$, hardly any angular correlations remain and also the radial order is lost. Particle transitions between different shells are revealed by a finite density in the radial regions between the shells[11].

Consider now a 3D Yukawa cluster with $N = 60$ particles, see figure 3. In the ground state (and at strong coupling), the particles are found in a configuration which has one particle in the centre, 15 particles on the inner shell and 44 particles

---

[10] The pair distribution function of finite clusters is computed by introducing discrete bins of width Δr, counting the average number of particle pairs with a distance in the interval $[r_{ij}, r_{ij} + \Delta r)$ and dividing by the bin volume.

[11] Note that, at very strong coupling, the correlation function in the region between two shells cannot be calculated since both ρ_2 and ρ_2^{uncorr} become zero.

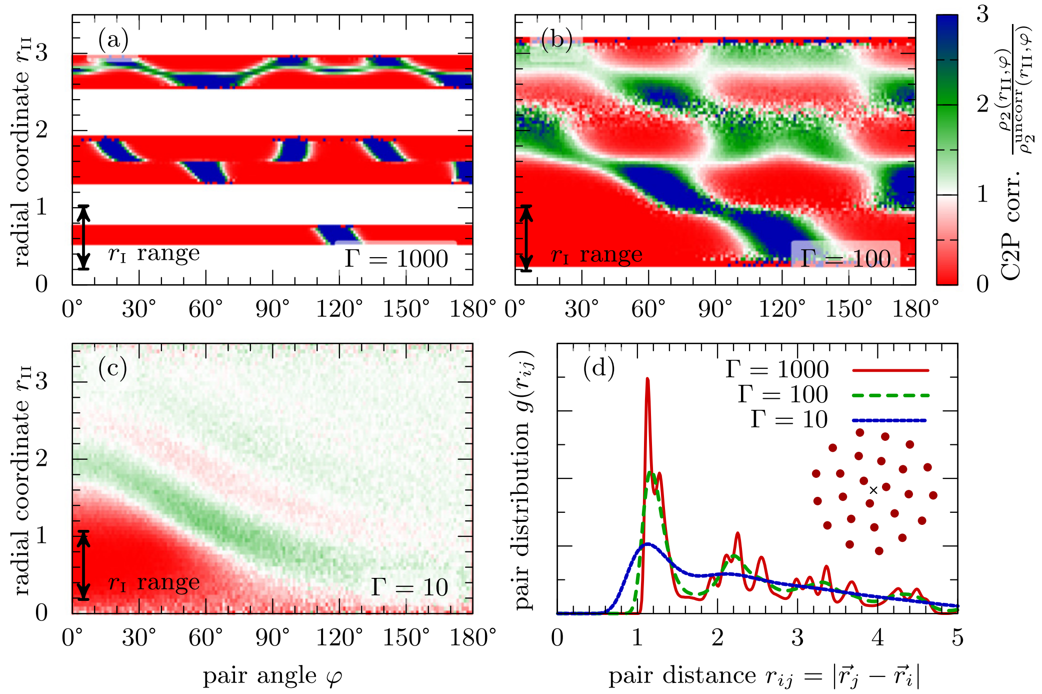

Figure 2. (*a*)–(*c*) C2P correlation function for a 2D Coulomb cluster with $N = 25$ particles for different coupling strengths. The ground state configuration consists of three concentric rings, see inset in (*d*). The first radial coordinate $r_{\rm I}$ is integrated over a range corresponding to the inner shell indicated by the arrows. Intra-shell correlations are visible at $r_{\rm II} \sim 0.7$ and $\phi = 120$. Pronounced inter-shell correlations with particles on the second shell are found at $r_{\rm I} \sim 1.6$ for strong coupling. (*d*) The radial pair distribution function $g(r_{ij})$ shows distinct peaks at high Γ which vanish when Γ is being decreased. Note that $g(r_{ij})$ decreases to zero at large distances for all couplings, due to the finite size of the cluster. Results are from a MC simulation, Γ is defined with the length unit $r_0 = [Q_{\rm d}/(4\pi\epsilon_0 m\omega_0)]^{1/3}$ as the characteristic pair distance.

on the outer shell (44-15-1). Again, one reference particle is chosen from the inner shell by integrating over $r_{\rm I}$. Due to the complexity of the particle composition on a spherical shell compared to the composition on a ring in 2D, the peaks at $r_{\rm II} \approx 1.2$, indicating intra-shell correlations, are not as sharp as for the 2D cluster at high coupling. Inter-shell correlations appear as dark and bright areas in the horizontal stripe at radius $r_{\rm II} \approx 2.4$ that corresponds to the outer shell. At moderate coupling, $\Gamma = 10$, the angular correlations are lost and frequent transitions between the shells take place as seen by the radial extension of the density.

2.5. Transport properties

Besides thermodynamic properties, also transport coefficients and their dependence on parameters like temperature or the magnetic field strength are important characteristics of dusty plasmas. A particularly important example of transport coefficients is the diffusion coefficient. In dusty plasmas, diffusion was investigated in detail in macroscopic systems, e.g. [128, 129] and references therein. In particular, in two dimensions an anomalous diffusion was found [130–133] which turned out to be a transient effect [134]. Furthermore simulations were performed for magnetized dusty plasmas. Here, the diffusion coefficient $D_\perp$ perpendicular to the magnetic field as well as the parallel diffusion coefficient $D_\parallel$ were found to be strongly affected by the magnetic field in the strong coupling regime approaching Bohmian diffusion (decay with B^{-1}) [129]. Recently diffusion in a 2D one- and two-component magnetized strongly coupled plasma was studied and interesting behaviour of the diffusion coefficients of both components was reported [135].

One way to compute (or measure) the diffusion coefficient in a macroscopic system is to use the mean square displacement (MSD)

$$u_r(t) = \left\langle |\vec{r}(t) - \vec{r}(t_0)|^2 \right\rangle_N = 2\,\dim\, D t^\alpha, \tag{5}$$

as an average over all N particles. Here dim is the system dimensionality (2 or 3) and α is the diffusion exponent which equals one for normal diffusion. However, the long time behaviour of the MSD has only limited meaning for mesoscopic systems since there the particles reach the cluster border after a few inter-particle distances [136].

Therefore, a different method is required to calculate the diffusion coefficients in small clusters. The instantaneous normal mode (INM) analysis has proven successful to this purpose [137–142]. This method deduces dynamic properties of a liquid state from the curvature of the energy landscape of the momentary configuration of the cluster. The first step is to calculate the dynamical (Hessian) matrix of the potential energy in the Hamiltonian, equation (3), as

$$\boldsymbol{A} = \left(\frac{\partial^2 E}{\partial r_{i\alpha} \partial r_{j\beta}} \right), \tag{6}$$

where i, j are particle indices and α, β indicate the (two or three) components of the coordinates. The eigenvalues of the this matrix present the squared eigenfrequencies ω_l^2 of the system. In a stable state, all these eigenvalues are

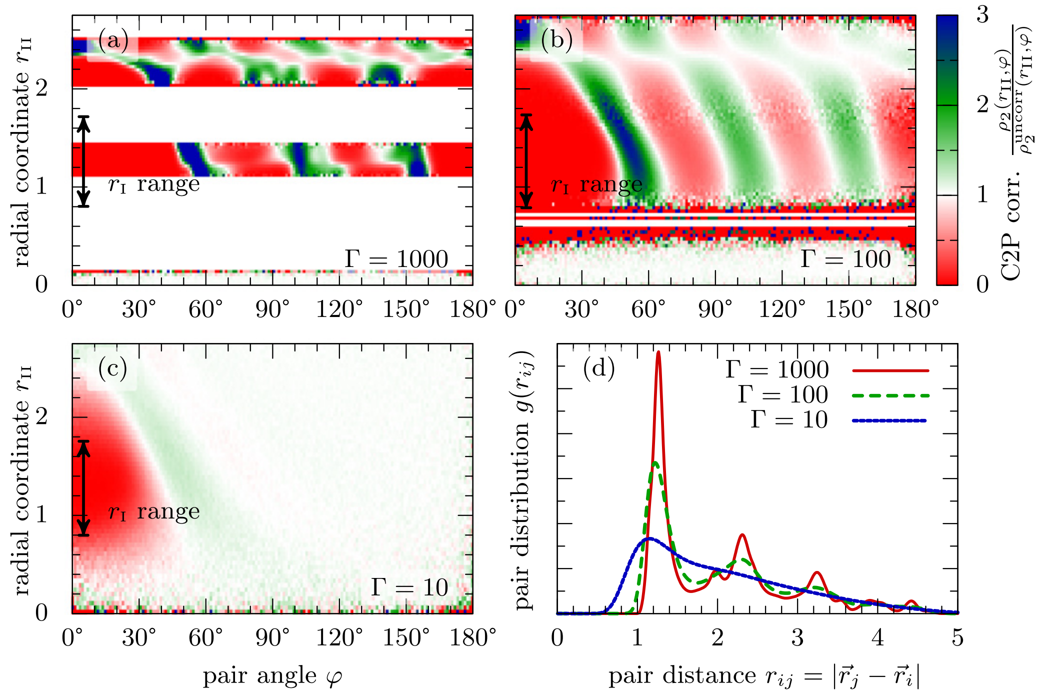

Figure 3. (a)–(c) C2P correlation function for a 3D Yukawa ($\kappa = 1$) ball with $N = 60$ particles for different coupling strengths. The ground state configuration consists of two concentric spherical shells and one particle in the centre. The first radial coordinate r_{I} is integrated over a range corresponding to the inner shell (arrows). *Intra-shell* correlations are visible at $r_{\mathrm{II}} \sim 1.3$. *Inter-shell* correlations with particles on the outer shell are visible at $r_{\mathrm{I}} \sim 2.2$ by the angular modulation of $g_2(r_{\mathrm{II}}, \varphi)$. ($d$) The radial pair distribution function $g(r_{ij})$ shows distinct peaks at high Γ which vanish when Γ is decreased. Note that $g(r_{ij})$ decreases to zero at large distances for all couplings, due to the finite size of the cluster. Results are from MC simulations, Γ is defined with the length unit $r_0 = [Q_{\mathrm{d}}/(4\pi\epsilon_0 m\omega_0)]^{1/3}$ as the characteristic pair distance.

positive resulting in real eigenfrequencies which reflect stable oscillations of the particles in the potential cage formed by their neighbours [143, 144]. A liquid instantaneous configuration, in contrast, has also negative eigenvalues of $\boldsymbol{A}$, resulting in purely imaginary eigenfrequencies reflecting unstable modes.

The second step is to calculate the spectral density, $\rho(\omega)$, which is normalized to unity, $\int \mathrm{d}\omega\rho(\omega) = 1$. In turn, we average over the normal modes of many configurations

$$\rho(\omega) = \left\langle \sum_{l=1}^{\dim\cdot N} \delta(\omega - \omega_l) \right\rangle. \tag{7}$$

This density is composed of a stable part, $\rho_{\mathrm{s}}(\omega)$, with real frequencies, and an unstable part, $\rho_{\mathrm{u}}(\omega)$, with imaginary frequencies. The unstable part $\rho_{\mathrm{u}}(\omega)$ is associated to a negative curvature in the momentary potential landscape. As described in [137–142], especially $\rho_{\mathrm{u}}(\omega)$ can be related to the diffusion constant. The self-diffusion constant is expressed as [137–142]

$$D = \frac{k_{\mathrm{B}}T}{m} \int \rho(\omega) \frac{\tau_{\mathrm{h}}}{1 + \tau_{\mathrm{h}}^2\omega^2} \mathrm{d}\omega, \tag{8}$$

and depends on the temperature $k_{\mathrm{B}}T$, the particle mass m and the average 'hopping time' τ_{h} for the transition across potential barriers between two local potential wells. This time is known as the inverse hopping frequency and calculated as

$$\tau_{\mathrm{h}}^{-1} = c \int \frac{\omega}{2\pi} \rho(\omega) A \exp\left(-B\frac{\omega^2}{k_{\mathrm{B}}T}\right) \mathrm{d}\omega, \tag{9}$$

where $c \approx 3$ is a constant taking into account the different routes to escape from a local potential minimum and the constants A and B are obtained from an exponential fit of $\rho_{\mathrm{u}}(|\omega|)/\rho_{\mathrm{s}}(\omega)$. For details, we refer the reader to [137–142].

3. Controlled change of the coupling strength by laser manipulation

3.1. General concept

In order to obtain valid information on thermodynamic properties it is essential to gain reliable control on the coupling parameter of the system. According to equation (1), three possibilities exist to control Γ: (i) controlling the charge Q_{d} of the particles, (ii) controlling the inter-particle distance b_{WS}, and (iii) controlling temperature T. With $\Gamma \sim Q_{\mathrm{d}}^2$, already a moderate variation of charge allows to change the coupling strength considerably. Thus, controlling the charge on the particles is the most tempting approach. However, this is not feasible in practice. Q_{d} is determined by geometric properties of the particles (such as the particle radius) and by the plasma conditions in the vicinity of the particles. Except for rare special conditions, the geometric properties cannot be altered during experiments and the local plasma conditions are not solely set by the discharge parameters but are modified by neighbouring particles as well. Thus, the charge is not directly controllable by means of external parameters such as discharge power, neutral gas pressure or bias voltages. Each will affect the plasma as well as the particle arrangement and thus result in a rather complex parameter dependence. Especially the inter-particle distance is strongly determined by the mutual particle repulsion, i.e. the particle charge, and the external confinement.

Thus, there is no easy access to control charge and inter-particle distance independently. Therefore, to decrease the coupling strength, temperature is the only remaining control parameter.

3.2. Kinetic and surface temperature of dust particles

Due to the macroscopic size of the particles (at least) two temperatures have to be distinguished: the kinetic temperature T^i of the particles and the particle surface temperature T_s^i, where 'i' labels different dust particles (we use the notion 'temperature' for the mean kinetic energy of the particle). To understand the physical difference of these temperatures we have to take a microscopic view point: The dust grains are solid bodies consisting of a very large number N of molecules (their atomic substructure and electronic properties are not relevant in this context). A transfer of energy to the particle from external sources will, in general, excite all $3N$ degrees of freedom of the molecules. Among them are 6 degrees of freedom ('centre-of-mass' (COM) modes) which are related to a collective displacement or a rotation of all particles which leave all inter-molecular distances unchanged. In contrast, the remaining $N-6$ degrees of freedom are related to intramolecular vibrations (phonons, 'relative modes'). It is easy to verify that the Hamiltonian of this system of N molecules can be split into a centre of mass and a relative part which are independent (they commute). Therefore, only the vibrations contribute to the surface temperature T_s^i. On the other hand, the kinetic temperature (energy) is connected only to the COM modes—in fact, only to the translational degrees of freedom. Now, in case of laser heating, predominantly the COM modes are excited via the radiation pressure, see the discussion in section 1.1. This is due to the large spot size compared to the intermolecular distances (in order to excite the relative modes there should exist a substantial field gradient on the scale of the intermolecular separation which is not the case). Still, an open question is to what degree individual photons are absorbed by the molecules which could lead to an excitation of the relative degrees of freedom and, eventually, to a slight increase of the surface temperature, but this effect will be neglected here.

The surface temperature is almost the same for all particles (provided they are under the same plasma conditions), $T_s^i \approx T_s$, because it arises from a very large number of coupled modes of many particles N. In contrast, the kinetic energies of individual particles (i.e. the individual T_i) are, in general, different. This is because the displacements of individual dust particles caused by lasers are, to a large extent, random, as is the case with the random displacements of the molecules of a gas. And as in the case of a gas, collisions between all dust grains eventually drive the system to thermodynamic equilibrium (with respect to the collective degrees of freedom). For a classical system one would expect that a Maxwellian velocity distribution is established, the width of which then reflects the overall kinetic temperature T. This expectation is fully confirmed by our simulations and the laser heating experiments discussed below, see figure 5.

The decoupling of centre of mass and relative degrees of freedom and, correspondingly, of T^i and T_s^i (and, therefore also T and T_s), has been verified–indirectly–experimentally. Here we mention detailed studies of the surface temperature by Maurer and Kersten [145] for dust particles doped with a temperature sensitive fluorescent dye. They concluded, from an energy balance model, that T_s^i scales roughly linearly with the rf power. At low rf discharge powers, T_s^i has been found slightly above room temperature. In contrast, in the experiments reported below, the kinetic temperature is found significantly higher than room temperature and thus it may strongly exceed T_s^i. This is because the radiation pressure from the laser(s) implies a substantial momentum transfer to the particles. Combined with their small weight and low friction in the plasma, these laser beams are capable to significantly accelerate individual dust particles.

Returning to our original goal—a control of Γ—we conclude that only the kinetic temperature has the meaning of thermodynamic temperature. (We mention that this holds rigorously only in the thermodynamic limit, however, many simulations and experiments indicate very similar behaviour in the case of finite clusters.) So, in the following we will concentrate entirely on the kinetic temperature T. We expect that variation of T (and hence Γ) gives access to the thermodynamic properties of finite dust clusters and to phase transitions. The only requirement which we have to fulfill is that the employed heating scheme should guarantee a truly random character of the individual kinetic temperatures T^i. In other words, the excitation should act like a thermostat for dust particles allowing for equilibration by particle scattering. As we will see below, properly chosen laser heating fulfills this requirement very well and allows for spatially homogeneous and stationary heating.

Finally we mention that, unlike T_s, the kinetic temperature T cannot be obtained experimentally from a conventional heat flux analysis. Recent investigations by Fisher *et al* [146] state that electrostatic fields in the plasma background provide a significant contribution to the kinetic temperature of dust particles. However, a complete understanding of the involved processes is still missing and this makes it difficult to control temperature this way. These questions are beyond the present review and are not crucial for our subsequent analysis. In the experiments discussed below, the kinetic temperature (kinetic energy) of individual particles is recorded directly by tracking all particles. This gives access to the collective properties of the COM degrees of freedom of the entire dust cluster, including the power specturm and the velocity distribution.

3.3. Realizing laser heating of dust particles

The idea to transfer momentum from a laser beam to a dust particle goes back to the early days of dusty plasma research [147–152] and has been used for many purposes so far. This includes the investigation of particle interaction potentials [63, 153, 154], the excitation of waves [147, 151], study of Mach cones [90, 91, 155, 156] or the stability and normal mode analysis [53]. The first systematic laser heating experiments were performed by Wolter and Melzer [92] and by Nosenko *et al* [93, 94]. In the experiment of Wolter and Melzer [92] the spot of a laser beam is rapidly moved via scanning mirrors to

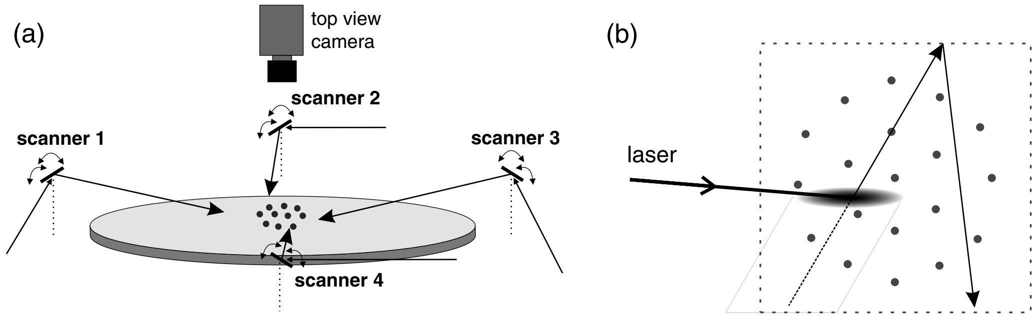

Figure 4. (*a*) Setup for a laser heating experiment using four laser beams. The spot of each laser beam is moved through the 2D plasma crystal layer by independently controlled the scanning mirrors. The scanned area is large enough to cover the entire crystal. The radiation pressure force impels the particles in the $\vec{e}_\parallel$ direction. (*b*) The improved heating method moves the spot at a constant speed in both directions until the border of the scanned area is reached. At this point, a new speed is chosen randomly for the inverse direction. Reproduced with permission from [96], Copyright 2012 AIP Publishing LLC.

one position in a 2D dust cluster and remains at this position for about one tenth of a second, accelerating dust grains during this time. Then, the laser spot is rapidly moved to the next randomly chosen position via galvanometer mirrors. A similar heating scheme has been developed in Greifswald in order to manipulate finite 3D clusters [97]. There, a laser beam is used to manipulate the cluster from the horizontal direction using this 'point and shoot' technique. In this experiment, a near Maxwellian velocity distribution of the particles is realized, but with different kinetic temperatures in the beam direction and perpendicular to it.

The experiment of Nosenko *et al* [93, 94] exploits two opposing laser beams which were directed onto a 2D plasma crystal using scanning mirrors. Driving these scanners with sinusoidal signals at an irrational frequency ratio a well defined area of the plasma crystal is scanned (i.e. heated) in a Lissajous figure-like fashion. In addition, the opposing beam setup assures that the transfered momenta cancel on average, while the kinetic energy of each particle is raised as a result of non-compensated momentum fluctuations. Nosenko *et al* showed that their laser heating results in a Maxwellian velocity distribution parallel and perpendicular to the optical axis. However, the temperature in perpendicular direction was found to be significantly lower. Obviously, the viscous damping of the neutral gas impedes that collisions redistribute sufficient energy in perpendicular direction.

To overcome this limitation recent laser heating experiments for 2D clusters use four laser beams, where each optical axis is equipped with two opposing beams and perpendicular orientation of both optical axes [96, 157], see figure 4(*a*). In addition, the scanning procedure has been optimized. The reason for this is that a scanning scheme based on Lissajous figures results in a velocity power spectrum where strong harmonics of the scanning frequencies are observed. This is an indication that the periodicity of the driver causes individual particles to move with the same periodicity, i.e. between two kicks of the laser the particle velocity decreases significantly. Therefore, the optimized scanning procedure (see figure 4(*b*)) assures that each particle is driven by a laser beam before its motion originating from the previous laser drive is damped out. Thus, the requirement that each spatial position is covered by the scanning procedure is only sufficient if the maximum time between two complete scans is less than the inverse of the damping rate.

The experiments of Schablinski *et al* demonstrated that this is feasible for small clusters ($N < 100$). Their measured velocity spectra show no residual peak of the scanning lasers. Figure 5 summarizes the basic features of their heating method. In figure 5(*a*) the velocity distributions of the heated system are clearly Maxwellian. Plot (*b*) stresses that the Maxwellian character is even obtained if the velocity distribution is checked for each particle individually. The small scatter in particle temperature is a clear indication that the heating process is spatially homogeneous. Therefore, the laser heating with four laser beams and an optimized scanning procedure can be regarded as an ideal thermostat for 2D dusty plasma crystals.

4. Theoretical description of 2D laser heating

In this section, we first describe how the 2D laser manipulation experiment described above is simulated with the Langevin molecular dynamics (LMD) method [96, 157, 158] and then develop an analytical model for the achieved temperature. We explicitly study the elaborate heating scheme used in the experiments that will be presented below in section 5.2. The purpose of such computer simulations is to suggest optimal values for the heating parameters and to recommend future experiments like inhomogeneous heating. Moreover, computer simulations provide the possibility to systematically scan single parameters like the heating power or the beam (spot) size at constant other parameters which is often experimentally too costly.

4.1. Langevin Molecular Dynamics simulations

In an LMD simulation, the Langevin equations of motion for the dust component

$$m\frac{\mathrm{d}\vec{v}_i}{\mathrm{d}t} = \vec{F}_i + \vec{f}_i^{\mathrm{L}} - \gamma m \vec{v}_i + \vec{\xi}_i(t), \quad i = 1\ldots N, \tag{10}$$

for all dust grains i are integrated numerically. In these equations, the first term on the right hand side results from minus the gradient with respect to $\vec{r}_i$ of the Hamiltonian, equation (3) (i.e. the forces due to external potentials and

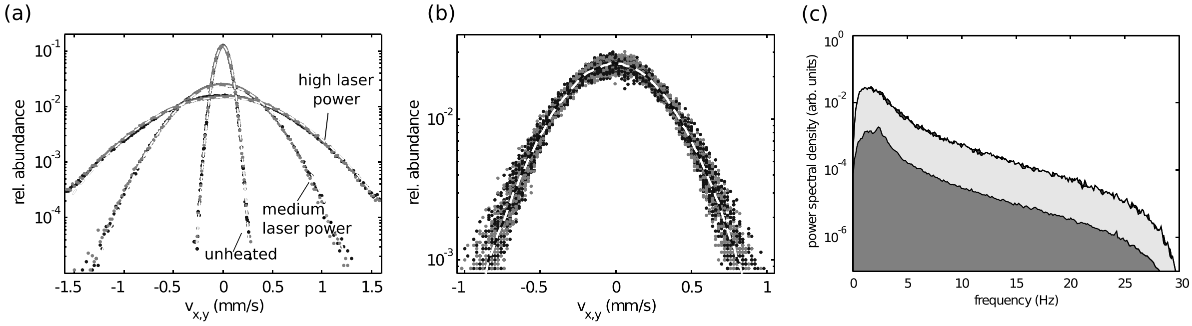

Figure 5. (*a*) Average particle velocity distribution function for a 2D cluster of 19 particles for three different values of the heating power. The velocity components in x and y direction (grey and black dots) are plotted separately. For each case (unheated, medium and high heating power) Gaussian fits (dashed lines) indicate only slight deviation from an ideal Maxwell distribution. (*b*) Velocity distributions for a heated system (similar to (*a*)), but here the distribution is calculated for each particle independently. The small scatter of the data confirms that all particles are heated equally. (*c*) Power spectrum of the velocity fluctuations. The spectrum of the unheated system is plotted in dark grey. The spectra of the x and y component of a heated system are plotted (light grey and black). Note that both components are equally heated and no artefacts from the scanning process can be found in the spectra. Reproduced with permission from [96], Copyright 2012 AIP Publishing LLC.

inter-particle interactions that appear in Newton's equations of motion). The last two terms on the right hand side describe the frequent collision of the dust grains with the neutral gas background statistically by a viscous damping force, $-\gamma m\vec{v}_i$, and a random force $\vec{\xi}_i(t)$. The random force has zero average and can be modelled by a Gaussian probability distribution with correlation function

$$\left\langle \xi_{i,\alpha}(t)\xi_{j,\beta}(t')\right\rangle = 2\gamma m k_{\rm B}T\delta_{i,j}\delta_{\alpha,\beta}\delta(t-t'), \qquad (11)$$

where i, j are particle indices and $\alpha, \beta \in \{1, 2\}$ indicate the spatial components of the random force vector. The amplitude of this force depends on the temperature $k_{\rm B}T$ as well as on the friction coefficient γ via the fluctuation-dissipation theorem (11).

The dust–dust interaction is described by a Yukawa potential, equation (2). In experiments on 2D clusters, the strong vertical confinement in the plasma sheath allows the formation of monolayer clusters. Therefore, the system is treated strictly 2D in the simulation.

The effect of the heating lasers on each particle is given by the second term on the rhs in equation (10), $\vec{f}_i^L = \sum_{l=1}^{N_L} \vec{f}_{il}^L$, which is composed of separate contributions of all N_L laser beams. The dominating effect of every single heating laser beam (index l) on particle 'i' is a momentum transfer by the radiation pressure which is described by the force $\vec{f}_{il}^L$. If the laser spot hits a dust grain, this particle is accelerated in beam direction. The laser force

$$F_l = q_{\rm optic}n_1\frac{\pi r_{\rm p}^2 I_{\rm laser}}{c} = q_{\rm optic}n_1\frac{\pi r_{\rm p}^2}{c}\frac{P_{\rm laser}}{2\pi\sigma_x\sigma_y} \times \exp\left[-\frac{\Delta_x^2}{\sigma_x^2}-\frac{\Delta_y^2}{\sigma_y^2}\right] \qquad (12)$$

is proportional to laser intensity $I_{\rm laser}$ at the particle position (Δ_x, Δ_y) relative to the laser spot centre, the cross-section of the dust particle $\pi r_{\rm p}^2$, the refractive index of the plasma n_1 surrounding the particle and a dimensionless quality factor $q_{\rm optic}$ [159]. This factor describing the momentum transfer by an incoming photon has the limiting values 1, if the particle was a perfect absorber, and 2 for a perfectly reflecting flat disk perpendicular to the beam. For a spherical particle reflecting, absorbing and transmitting photons it is $q_{\rm optic} < 2$. Typical values of $q_{\rm optic} \approx 1$ are reported for melamine particles [159]. $\sigma_{x,y}$ characterizes the extensions of the elliptical spot which has an area of $2\pi\sigma_x\sigma_y$.

As sketched in figure 4, the laser beams strike the cluster from above the levitation plane with a low angle of incidence. The out-of-plane component of the accelerating force is considered to have no impact on the particles' motion due to the strong vertical confinement. However, the spot profile is stretched in beam direction due to the relatively small angle of incidence, $\alpha < 90°$. The laser force is time and space dependent according to the experimentally chosen scheme. The amplitude of the force depends on the particle's position inside the spot which is described by an anisotropic Gaussian intensity profile. The force acting on a particle at position $\{\Delta_x(t), \Delta_y(t)\} = \vec{r} - \vec{r}_l(t)$ away form the moving spot centre is described by

$$\vec{f}_l(\vec{r}, t) = \frac{P_0}{2\pi\sigma_x\sigma_y}\cdot\exp\left[-\frac{\Delta_x^2(t)}{2\sigma_x^2}-\frac{\Delta_y^2(t)}{2\sigma_y^2}\right]\vec{e}_l, \qquad (13)$$

where $\vec{e}_l$ is a unit vector in beam direction. Here, based on equation (12), we have introduced dimensionless units for all lengths and P_0. The amplitude of the force $P_0 = q_{\rm optic}n_1\pi r_{\rm p}^2 P_{\rm laser}/c$ is determined by the laser power, the cross section of the dust grain and its absorption and reflection characteristics. Since only the in-plane component has an effect on the particle's motion, P_0 is reduced by the factor $\cos\alpha$ where α is the angle of incidence. The trajectories of the laser spot centres within the levitation plane are denoted by $\vec{r}_l(t) = \{x_l(t), y_l(t)\}$ and depend on the heating scheme.

4.2. Comparison of different heating schemes

All investigated heating methods (a more extensive analysis was reported in [157, 160]) use triangular signals to drive the x- and y-oscillations of the lasers spots $x(t) = x_0\cdot{\rm triag}(f_x t)$, $y(t) = y_0\cdot{\rm triag}(f_y t)$. Using a sinusoidal signal would cause

Table 3. Parameters defining the pattern which is scanned by the lasers. Since both beams are oriented in the ±x-direction for method A-I, $f_{\parallel} = f_x$ in that case.

method	A-I	B
laser beams	2	4
frequency ratio	pseudo-irrational	random frequencies
$f_{\parallel}$	14.5623 Hz	50–300 Hz
$f_{\perp}$	9.0 Hz	15–60 Hz

an increased intensity at the borders of the scanned area. The heating methods differ in the scanning frequencies f. These frequencies are fixed for the heating method A-I. Method A-I uses the same frequencies for both laser and a pseudo-irrational ratio f_x/f_y. For method B, the scanning frequencies are dynamically changed each time a laser spot reaches the border of the scanned area. Hence, no pattern is repeated [96, 157]. added. The parameters of all heating methods are summarized in table 3 and the scanned patterns are shown in figure 6.

For the simulation results presented in this review, we used the following dimensionless units of length, time and energy: $r_0 = [Q_{\rm d}^2/(4\pi\varepsilon_0 m\omega_0^2)]^{1/3}$, $t_0 = \omega_0^{-1}$, and $E_0 = [Q_{\rm d}^4 m\omega_0^2/(4\pi\varepsilon_0)^2]^{1/3}$. For the numerical integration of the stochastic differential equations, we used an integration scheme described by Mannella *et al* that can be considered as an extension of the 'leap frog' scheme [161]. For details concerning the simulations, we refer the reader to [157, 158]. (This scheme can also be easily generalized to incorporate homogeneous magnetic fields of arbitrary strength [162–164]).

As a first result, our LMD simulations confirmed the importance of randomly changing the scanner frequency. Especially rational scanning frequency ratios f_x/f_y which result in a closed scanning pattern prove to be problematic. A second result is the confirmation of the excellent heating qualities (with respect to homogeneity of the heating) of the random frequency method B [157]. While constant scanning frequencies and combinations of them appear as peaks in the power spectral density (PSD) of the particle velocities for the method A-I, this artefact is removed by randomly changing the scanning frequencies, see figure 7 and figure 5(c). The PSD further discloses that effective energy transfer from x- to y-motion works for low frequencies, $f \lesssim 8\,$Hz, only. The pseudo-irrational frequency method A-I shifts the entire spectrum of the motion in x-direction to higher energies but also induces several peaks at the scanner frequencies and combinations thereof, figure 7(a).

Both experiment, figure 5(c), and LMD simulation, figure 7 (bottom), show that the random frequency method B is well suited as a thermostat for the 2D dust system. The energy input is homogeneous over the entire frequency spectrum. It is also homogeneous in space and the Maxwellian shape of the velocity profile is conserved in both x- and y-direction. Moreover, the random frequency method B is very robust against changes in the laser parameters [157]. The temperature increase ΔT (i.e. the heating effect) is reduced when the typical scanning frequency $\bar{f}$ of the laser beams is increased according to $\Delta T \propto \bar{f}^{-1}$. However, in order to achieve a thermal heating effect, each particle should frequently be affected by a laser spot. This condition is violated for $\bar{f}$ below the trap frequency ω_0. Therefore, scanning frequencies of the order of a few ω_0 are advantageous [157].

4.3. Analytical estimate for the temperature increase

We now derive an analytical approximation for the heating power as a function of the laser parameters: the force amplitude P_0, spot size $\sigma_{x,y}$, size of the scanned array $2X \times 2Y$ and average spot velocity. The spot velocity is connected to the scanning frequencies, $f_{l,x}$, $f_{l,y}$, via $v_{l,x} = 4Xf_{l,x}$ and $v_{l,y} = 4Yf_{l,y}$. A similar analytical derivation of the heating effect was performed by Wolter and Melzer for a setup with one laser spot that was rapidly moved to one position, remained there for a dwell time of a few microseconds and was then moved to the next position [92].

Here we extend this model to a continuously moving laser spot corresponding as closely as possible to the experimental heating method by Schablinski *et al* that is discussed in section 5. For simplicity, the momentum transfer is computed in one direction only. Since the velocity of the dust is small compared to the velocity of the moving laser spot, the particle's displacement during an acceleration event can be neglected. The time-dependent force acting on a particle when a spot passes with distance Δy_0 in y-direction is

$$F(t') = \pm P_0 \frac{1}{\sqrt{2\pi}} \mathrm{e}^{-\frac{t'^2}{2\tau^2}} \cdot \underbrace{\frac{1}{\sqrt{2\pi}} \frac{1}{\sigma_x\sigma_y} \exp\left\{-\frac{1}{2}\left[\frac{\Delta y_0^2}{\sigma_y^2} - \tau^2 \frac{\Delta y_0^2 v_y^2}{\sigma_y^4}\right]\right\}}_{:=\Sigma}, \tag{14}$$

where we introduced the time scale of the passing event $\frac{1}{\tau^2} = \frac{v_{l,x}^2}{\sigma_x^2} + \frac{v_{l,y}^2}{\sigma_y^2}$, and the shifted time $t' = t + \tau^2 \frac{\Delta y_0 v_{l,y}}{\sigma_y^2} - t_0$. Here, t_0 is the time when the spot has the smallest distance Δy_0 in y-direction and we introduced the time-independent geometry factor Σ. The total momentum transfer to the particle during this laser hit follows from equation (14)

$$\Delta p = \int_{-\infty}^{\infty} \mathrm{d}t'\, F(t') = \pm P_0 \Sigma \cdot \tau, \tag{15}$$

and is cancelled, on average, by the momentum transfer from the opposing laser beam. To calculate the average energy transfer, we need to average the squared geometry factor Σ^2 over all possible passing distances Δy_0. Assuming that the particle at $(x_{\rm p}, y_{\rm p})$ does not come too close to the boundary, the integration limits can be extended to infinity, with the result

$$\left\langle \Sigma^2 \right\rangle_y \approx \frac{1}{2Y} \cdot \frac{1}{2\sqrt{\pi}} \cdot \frac{1}{\sigma_x\sigma_y} \cdot \frac{1}{v_{l,x}} \cdot \frac{1}{\tau}. \tag{16}$$

Each time the laser crosses the levitation plane in x direction, it passes the particle position once. Then, the 'passing rate' χ is given by the inverse crossing time in x direction as $\chi = \frac{v_{l,x}}{2X}$.

The energy change of a particle with velocity v during a single laser–particle interaction event is (neglecting the deceleration due to friction during the kick),

$$\Delta E = E' - E = v\Delta p + \frac{\Delta p^2}{2m}, \tag{17}$$

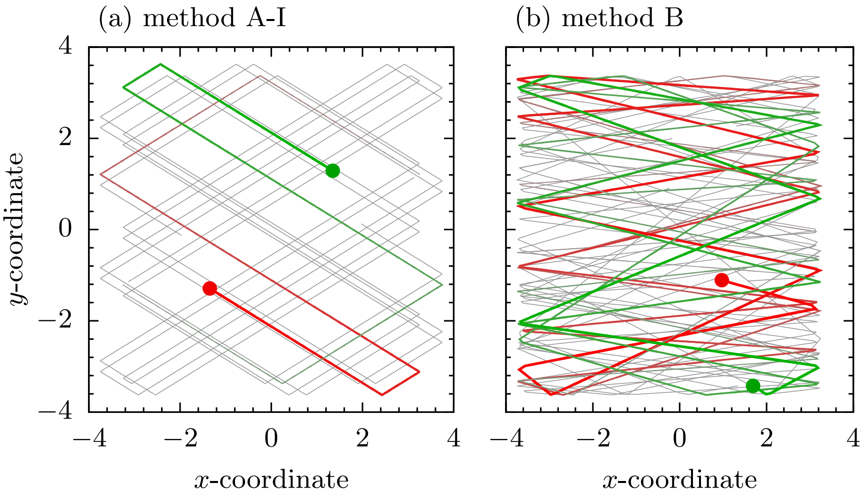

Figure 6. Trajectories of the laser spots (red/green: ±x-direction) for two of the investigated heating methods. (a) Method A-I uses a pseudo-irrational frequency ratio. (b) Using method B, a new scanning frequency is randomly chosen each time a laser spot reaches the border. Here, the two additional spots of the laser oriented in the ±y-direction are omitted, for the sake of clarity.

where the momentum transfer Δp is given by equation (15). From this the average energy transfer is obtained using equation (16),

$$\langle \Delta E\rangle = \frac{1}{2m} P_0^2 \Sigma^2 \cdot \tau^2, \tag{18}$$

which depends on the passing distance Δy_0 via Σ. Then, the average energy transfer per time follows from averaging over Δy_0, multiplying by χ and using equation (16),

$$\left\langle \frac{\Delta E}{\Delta t}\right\rangle = \frac{1}{2m}\cdot\frac{1}{2\sqrt{\pi}}\cdot P_0^2\cdot\frac{1}{4XY}\cdot\frac{1}{\sigma_x\sigma_y}\cdot\tau_{\mathrm{eff}}, \tag{19}$$

where we also took into account that the laser spot velocity components v_x, v_y vary in the experiment by computing an effective time scale τ_{eff} by averaging $\tau(v_{l,x}, v_{l,y}) = (v_{l,x}^2/\sigma_x^2 + v_{l,y}^2/\sigma_y^2)^{-1/2}$ over all possible spot velocities $v_{l,x} \in [v_x^{\min}, v_x^{\max}]$ and $v_{l,y} \in [v_y^{\min}, v_y^{\max}]$[12].

From the result (19), we can now calculate the equilibrium temperature T_{eq} in the Langevin MD model which follows from the balance between laser input power P_{laser}, the power input by the stochastic force, $P_{\mathrm{stochastic}}$, and the power loss due to friction, P_{friction},

$$P_{\mathrm{laser}} + P_{\mathrm{stochastic}} + P_{\mathrm{friction}} = 0. \tag{20}$$

Assuming a 1D Maxwellian particle velocity distribution with temperature T_{eq},

$$p(v) = \sqrt{\frac{m}{2\pi k_{\mathrm{B}} T_{\mathrm{eq}}}}\,\mathrm{e}^{-\frac{mv^2}{2k_{\mathrm{B}}T_{\mathrm{eq}}}}, \tag{21}$$

and the velocity change due to friction, $\dot{v} = -\gamma v$, where γ is the friction coefficient, we obtain

$$P_{\mathrm{friction}} = \left\langle \frac{\mathrm{d}}{\mathrm{d}t}\frac{m}{2}v^2\right\rangle = -m\gamma\left\langle v^2\right\rangle = -\gamma k_{\mathrm{B}} T_{\mathrm{eq}}. \tag{22}$$

On the other hand, in an equilibrium system without laser heating at the temperature T_0 of the neutral gas, the power loss due to friction is be compensated by $P_{\mathrm{stochastic}} = \gamma k_{\mathrm{B}} T_0$.

Using equation (20) and the power input by the laser from equation (19) multiplied by 2 to take into account the pair of lasers in each direction, we obtain our final result for the equilibrium kinetic temperature of the dust particles

$$T_{\mathrm{eq}} = T_0 + \frac{\sqrt{\pi^3}}{2m\gamma k_{\mathrm{B}}}\cdot I_0^2\cdot\frac{\sigma_x\sigma_y}{XY}\cdot\tau_{\mathrm{eff}}, \tag{23}$$

where we introduced the laser intensity according to $I_0 = P_0/(2\pi\ \sigma_x\sigma_y)$. It is interesting to note the dependence on the relevant system parameters: T_{eq} grows proportional to the square of the laser intensity, in agreement with the findings of Wolter and Melzer [92], and the ratio of spot area to scan area and inverse proportional to the neutral gas friction. These qualitative trends are also seen in the experiments. The time scale τ_{eff} introduces additional slightly more complex dependencies[13].

Despite the simplicity of the model, the accuracy of the result (23) is very good, as is confirmed by comparison to LMD simulations, see table 4. The temperature is overestimated slightly, and the accuracy improves with γ from about 15% to better than 10%. For very small spot sizes and low friction (not shown) the agreement is even better than 5%. For very large spot sizes, $\sigma_x \gtrsim 0.7$ in dimensionless units, the formula becomes less accurate. Then, most particles are close to the border of the scanned area compared to the spot width, violating the assumption of equation (16). Moreover, τ_{eff} becomes large in this case and the deceleration due to friction as well as the interaction with other particles during the hitting event should not be neglected.

Our result is not only in very good agreement with the simulations, it is also useful for characterizing the heating in the experiment. In fact, the spot size used in table 4 is typical

---

[12] The integral in the expression for the effective time scale can be solved using Mathematica.

[13] τ_{eff} is inversely proportional to the spot velocity, when both $v_{l,x}$ and $v_{l,y}$ intervals are scaled by the same factor. Increasing the laser scanned area has the side effect of decreasing τ_{eff} via the faster spot velocity at constant scanner frequencies. Therefore, the temperature increaes scales as $\Delta T = T_{\mathrm{eq}} - T_0 \propto X^{-3}$ with the side length of the scanned area. At constant aspect ratio $\sigma_x : \sigma_y$, the passing time τ_{eff} scales linearly with σ_x.

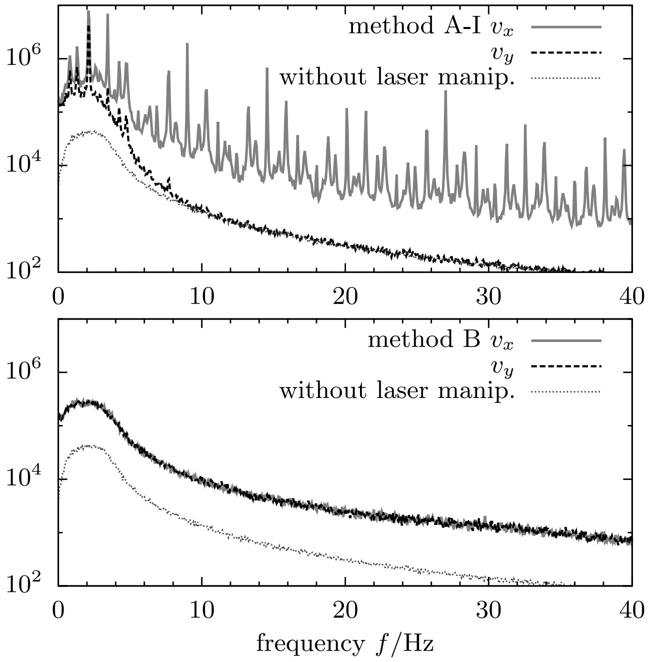

Figure 7. PSD of the dust velocity averaged over all particles of a Yukawa cluster with $N = 38$ particles with different heating methods (trap frequency $\omega_0 = 5.5\,\mathrm{s}^{-1}$). Top: method A-I uses one pair of laser beams in the $\pm x$-direction and a pseudo-irrational scanning frequency ratio f_x/f_y. Bottom: heating method B uses two pairs of laser beams to accelerate the particles in both $\pm x$- and $\pm y$-directions. The scanning frequencies are randomly chosen each time the border of the scanned area is reached. The spectra for v_x and v_y coincide, here. Only this method conserves the shape of the PSD by shifting the entire spectrum to higher energies.

Table 4. Comparison of equation (23) and results from a LMD simulation. Deviations refer to the value of Gamma (lines marked γ. The second lines show the associated temperature T). For smaller spots (not listed), the agreement is even better. Parameters: particle number $N = 25$, screening parameter $\kappa = 1$, coupling parameter without laser heating $\Gamma_0 = 200$, trap frequency $\omega_0 = 5.5\,\mathrm{Hz}$, dimensionless laser power $F_0 = 10$, scanned area $X = Y = 3.5$.

γ	Formula	Simulation	Deviation	
	$\sigma_x = 0.50$, $\sigma_y = 0.10$			
0.67	53.23	63.17	15.7%	Γ
	18.79×10^{-3}	15.83×10^{-3}		T
1.00	70.24	80.26	12.5%	Γ
	14.24×10^{-3}	12.46×10^{-3}		T
1.33	83.71	94.52	11.4%	Γ
	11.95×10^{-3}	10.58×10^{-3}		T
1.66	94.65	104.7	9.60%	Γ
	10.56×10^{-3}	9.550×10^{-3}		T
2.00	104.0	114.5	9.22%	Γ
	9.619×10^{-3}	8.732×10^{-3}		T
2.33	111.6	121.5	8.15%	Γ
	8.965×10^{-3}	8.234×10^{-3}		T
2.66	118.0	127.7	7.57%	Γ
	8.473×10^{-3}	7.831×10^{-3}		T

for the experiments. Assuming that the visible spot width is $\Delta_{\mathrm{vis}} = 3\sigma$, our formula suggests a coupling strength of $\Gamma^{\mathrm{form}} = 80$ which is in good agreement with the measured temperature $T = 3.5\,\mathrm{eV}$ corresponding to $\Gamma^{\mathrm{exp}} = 63$ for the maximum laser power used in *et al* [96]. However, that result has to be understood as a rough approximation, since parameters like the spot size, the trap frequency, and laser power losses in the optical setup each have an uncertainty of several percent in the experiment.

5. Experimental results for 2D dusty plasmas

We now turn to the experiments on laser heating. First, we start with 2D systems and continue, in section 6, with experiments with finite 3D dust cluster. Before presenting our experimental results for finite 2D dust clusters we briefly summarize previous work on extended systems.

5.1. Experimental results for extended systems

In many experiments in extended 2D systems the Lissajous heating scheme A-I (see section 4.2) has been applied since it allows one to densely scan (and heat) a well defined dust area. This technique has been used successfully to drive 2D extended dust systems into the liquid state [94, 165, 166]. There, it has been demonstrated that the defect concentration in steady-state laser-heating experiments exhibits an Arrhenius-type dependence on the kinetic temperature [165]. Moreover, these experiment suggest a grain-boundary-induced melting scenario which is also observed in non-equilibrium heating experiments, e.g. by changing the gas pressure of the plasma discharge [17].

Further, experiments on heat transport and particle transport properties, such as diffusion and viscosity, of laser-heated dust layers have been performed, see e.g. [89, 94, 167–170]. From these, fundamental transport parameters like the thermal diffusivity of the dust component, as well as diffusion constants, Γ-dependent viscosities and anomalous diffusion properties have been identified and measured. These experiments have yielded important information on the application of laser–dust interaction methods in the field of dusty plasmas which are of high relevance also for strongly correlated small dust clusters at finite temperature.

5.2. Experimental results for 2D clusters

The remainder of this section will concentrate on finite 2D clusters and their thermodynamic properties. Especially the phase transition of these small systems is of interest as it should significantly depend on the cluster size. The following experiments use the isotropic heating method B of Schablinski *et al* [96, 157], which has been introduced in section 4.2. As shown there, the laser heating effectively provides a heat bath for the dust particles assuring that the dust subsystem is in thermodynamic equilibrium. Changing the laser power will result in a different temperature of this thermostat. In the experiment, for each temperature, long time series are recorded to obtain the trajectories of all particles. Examples of such particle trajectories are shown for low, medium and high temperature in figure 8(a). For low temperature the particles are well localized and only a slight angular rotation is observed. At medium temperature the particles are less localized in angular direction. Finally, at high temperatures

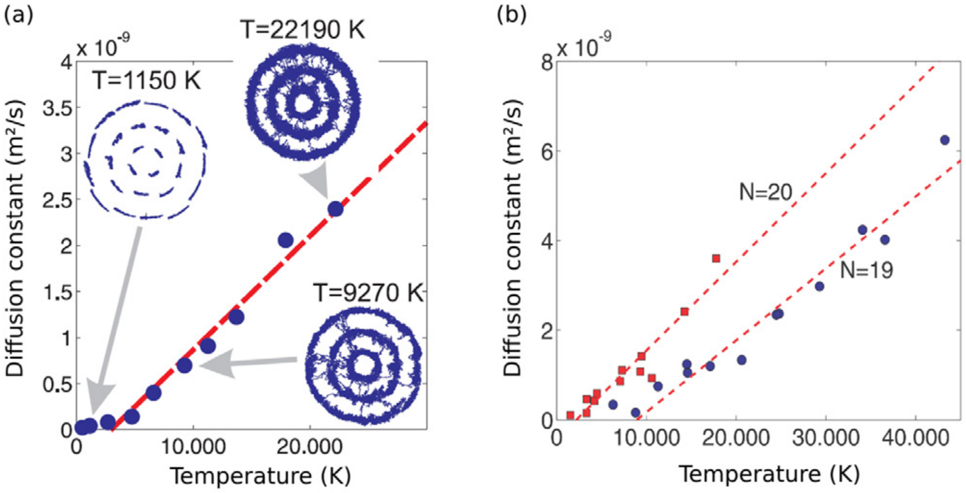

Figure 8. Diffusion constant as a function of temperature for finite 2D clusters. (*a*) Above a critical temperature the diffusion constant increases linearly with temperature. The insets show trajectories of a dust cluster with $N = 26$ particles at different temperatures. (*b*) Diffusion constant for two different dust clusters. The $N = 19$ cluster with its (1-6-12) shell occupation is highly symmetric and its critical temperature is significantly higher than that of the less symmetric $N = 20$ cluster. Part (*a*) reproduced with permission from [142]), Copyright 2013 The American Physical Society. Part (*b*) reproduced with permission from [171], Copyright 2012 The American Physical Society.

(high laser power), the radial correlations vanish as well. Thus, we confirm that the melting process has two phases: first, a loss of angular correlation and, second, a loss of radial correlation [51, 171].

To determine the melting temperature several methods have been proposed (see [172] and references therein). Unfortunately most of them either fail for small clusters or are experimentally not feasible since they require extremely long time series in order to achieve sufficient statistics, see section 2.3. Therefore, recently different methods have been applied which were introduced in sections 2.4, 2.5: The first is the INM analysis. This method computes the frequencies of the eigenmodes of a cluster from the eigenvalues of the dynamical matrix, see section 2.5. The results of such an INM-analysis are plotted in figure 8. The plots show that, above a critical temperature, the diffusion constant increases linearly with temperature. A freezing temperature can be derived approximately from the point where D vanishes [144]. Thus one can estimate a melting temperature T_{M} by extrapolating the $D(T)$ curve toward zero. Especially in figure 8(*b*) the comparison of a highly symmetric cluster ($N = 19$) and a cluster with low symmetry ($N = 20$) reveals that the melting temperature of the symmetric cluster is significantly higher ($T_{\mathrm{M}}^{19} \approx 9.000\,\mathrm{K}$, $T_{\mathrm{M}}^{20} \approx 2.000\,\mathrm{K}$). A systematic investigation of melting temperatures as a function of particle number [142] has shown that symmetry has a mayor influence on melting temperatures of finite systems, confirming earlier theoretical predictions [51, 125].

The above results show that the INM analysis is sensitive to the cluster symmetry. However, it does not resolve different melting processes such as inter-shell and intra-shell melting. (For example, it is well known [51] that the above two clusters have angular melting temperatures that differ by many orders of magnitude but that their radial melting temperatures are comparable.) For this reason, we also consider the C2P correlation function (see section 2.4) for the experimental cluster of 19 particles. Figure 9(*a*) shows a highly ordered structure of the weakly manipulated cluster. The inner shell is occupied by six particles. Intra-shell neighbours are found under angles of $\varphi = 60^\circ$, 120° and 180°, as is clearly seen by the peaks at these angles and a radius $r_{\mathrm{II}} \approx 1\mathrm{mm}$, corresponding to the inner shell. The outer shell is occupied by 12 particles and the angular order with respect to the inner shell is fixed. Distinct peaks are visible at multiples of $\varphi = 30^\circ$. When the laser power is increased to a moderate value (see figure 9(*b*)), clear intra-shell and inter-shell correlations persist. However, inter-shell rotation ('angular melting') has started, as the peaks at the outer radius are no longer fully separated. At the inner shell radius, weak peaks at $\varphi \approx 103^\circ$ and $\approx 154^\circ$ (arrows in figure 9(*b*)) indicate the occurrence of configurations with seven particles on the inner shell. The appearance of this metastable configuration indicates the onset of radial melting. Finally, at high laser power (figure 9(*c*)), the correlations between inner and outer shell have vanished almost completely. At this heating power, the frequent particle transitions between the two shells give rise to a finite density in the region between these shells.

Thus the C2P correlation function fully confirmed the stability of this 'magic number' cluster against inter-shell rotation. Yet a complete quantitative analysis of the different melting temperatures and their dependence on the particle number is still open.

6. Experimental results for 3D clusters

3D dust clusters are formed in parallel plate radio-frequency (rf, 13.56 MHz) discharges, see figure 10 and e.g. [55, 120, 173, 174]. The discharges are typically operated in argon at gas pressures between 1 and 100 Pa and at rf powers between 1 and 10 W. The dust grains trapped in the discharge generally

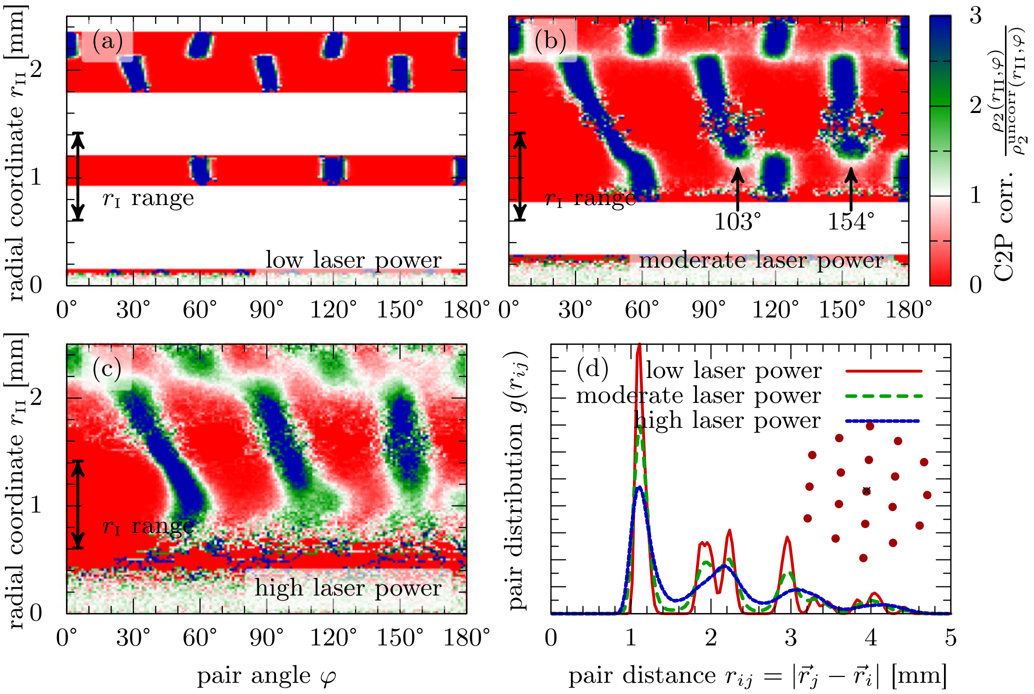

Figure 9. (*a*)–(*c*) C2P correlation function for a laser heated cluster of $N = 19$ particles. The low laser power corresponds to T=2.800 K, the moderate (high) power to T=17.000 K ($T = 34.000$ K). The first radial coordinate is averaged over the inner shell (arrow). (*d*) Radial pair distribution function for all three laser powers. Note that it does not distinguish between different shells. The inset shows the cluster configuration at the lowest laser power.

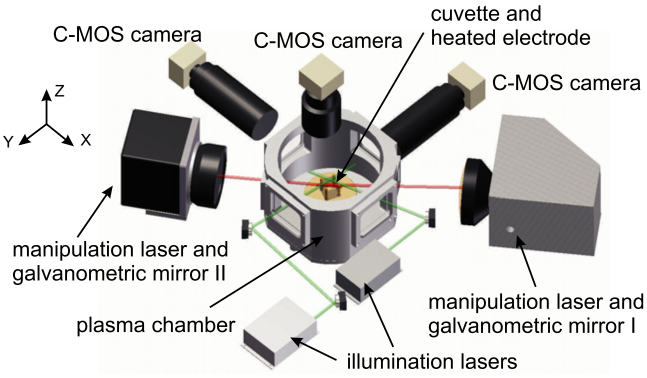

Figure 10. Sketch of the experimental setup to investigate laser heated 3D dust clusters. The particles are trapped in the cubic glass box and are illuminated by two Nd : YAG lasers from two sides and heated by two diode lasers from opposite directions. The three orthogonal high-speed cameras allow to trace the full 3D particle motion individually. From [175].

are monodisperse plastic microspheres with diameters chosen between 3 and 10 μm. These 3D clusters are trapped inside a cubic glass cuvette placed onto the lower electrode. The glass box provides inward electric forces on the negative dust grains. To compensate the gravitational force an upward thermophoretic force is applied by heating the lower electrode. The combination of all forces provides a 3D harmonic confinement [106]. There, the particles arrange in nested spherical shells forming Yukawa balls or Yukawa clusters [55, 120, 176], see section 2.2.

In the experiments described here, the particles are illuminated by low-intensity laser beams and the scattered light is recorded with high-speed video cameras at frame rates of 50 to 200 frames per second (fps), typically [97, 120, 176, 177]. For the observation of the 3D clusters a stereoscopic camera setup [120] is used where the particles are observed from three orthogonal directions. This setup allows to measure and reconstruct the full 3D trajectories of clusters with up to $N = 100$ particles with high temporal resolution [120, 178]. Consequently, the dynamical properties of the dust cluster can be followed for all particles individually. To realize a heating process for these 3D clusters a simpler approach than for the 2D case had to be chosen due to experimental constrains. The transfer of the elaborate heating schemes used for the 2D clusters (section 5.1) to the 3D case would require six beams, two of which would be blocked by the electrodes. Here, only two additional opposing laser beams are oriented parallel to the electrode and are randomly swept over the cross section of the cluster with a dwell time of $\tau = 0.1$ s at each position [97, 175, 177]. The two laser beams at 660 nm wavelength are operated with up to 1 W output power. The random ‘kicks’ to the particles by the radiation pressure mimic a heating process for these 3D clusters.

As a consequence, the resulting velocity distribution of the particles in the cluster is only near-Maxwellian, with an overpopulation of ‘cold’ dust particles [97]. Also the heating is more effective in the direction of the beams resulting in higher temperatures along this axis. Consequently, this laser-heating scenario of 3D clusters does not provide a true thermodynamic heating, yet. Nevertheless, from the velocity distributions reasonable kinetic temperatures $kT_\alpha = m\langle v_\alpha^2\rangle$ with $\alpha = x, y, z$ can be assigned and values of the order of a few times 10^4 K (few eV) have been realized by this laser heating setup.

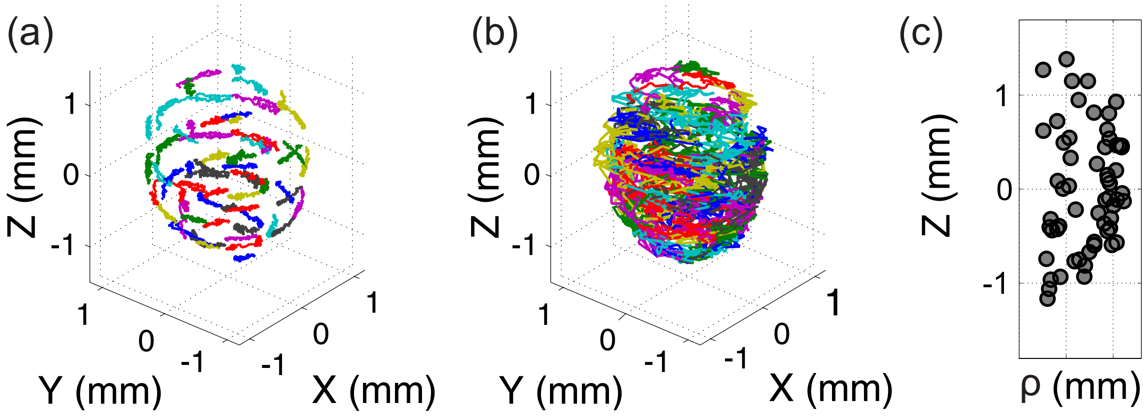

Figure 11. Trajectories of a $N = 60$ particle cluster recorded over a time span of about 10 s. (*a*) Without laser excitation, (*b*) with 250 mW laser power. (*c*) Equilibrium particle positions in cylindrical coordinates $\rho = \sqrt{x^2 + y^2}$ and z for the unheated case (*a*). From [175].

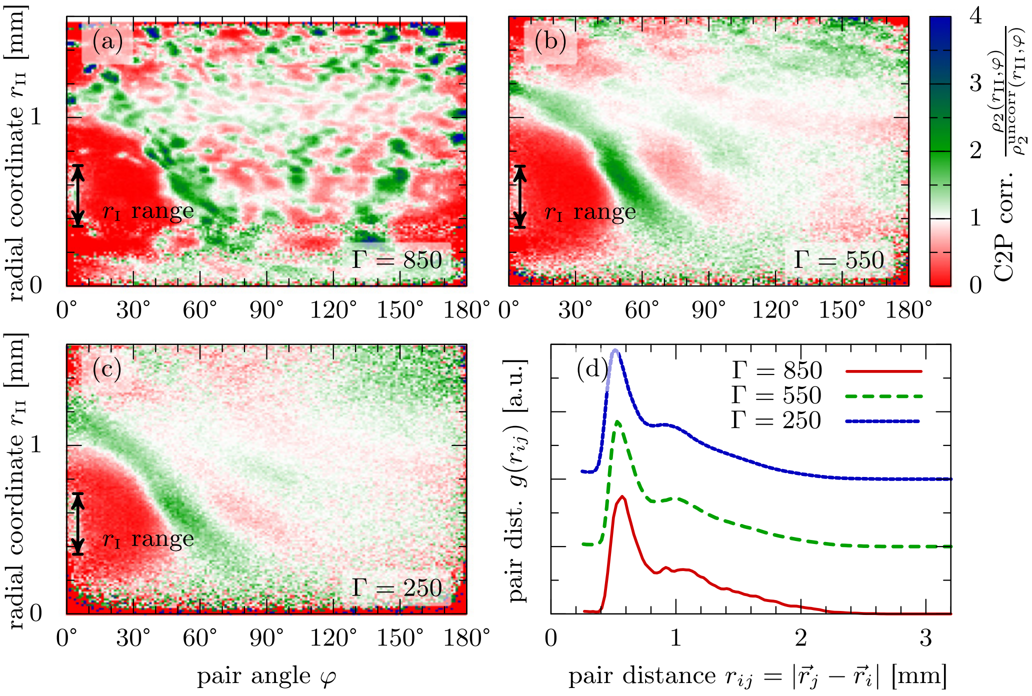

Figure 12. C2P correlation functions for the $N = 60$ cluster, (*a*) without laser heating ($\Gamma = 850$), (*b*) for a laser heating power of 100 mW ($\Gamma = 550$) and (*c*) 300 mW ($\Gamma = 250$). (*d*) Pair distribution function. The smoothening of the curve with decreasing Γ indicates the loss of order but, in contrast to the C2P correlation function in (*a*)–(*c*), the pair distribution function cannot distinguish intra-shell from inter-shell correlations. (The zero line is shifted for $\Gamma = 550$ and $\Gamma = 250$, for sake of clarity).

Here, as an example, the heating and melting of a 3D cluster with $N = 60$ particles is demonstrated[14] using the pair of opposing heating laser beams. The Yukawa ball is spherical in shape and consists of two shells, see figure 11. By increasing the laser power, the amount of heating is increased and melting is achieved. For low laser heating power the cluster remains in a solid-like arrangement, as seen from the particle trajectories. Stronger random particle motion is excited at higher laser power where then frequent intra-shell and inter-shell particle exchanges are seen. Hence, the cluster is apparently driven into the liquid regime. The change of structural and thermodynamic properties that is induced by the lasers is illustrated in figure 12(*d*). There we show the pair distribution function $g(r_{ij})$ for three different heating powers. The differences in $g(r_{ij})$ between the three heating powers are only small. All three curves show a pronounced first-neighbour maximum at $r_{ij} \approx 0.6$ mm, a shoulder at $r_{ij} \approx 1.2$ mm corresponding to second neighbours and a decay to zero. While the curves for $\Gamma = 250$ and $\Gamma = 550$ appear smooth, a substructure is visible at high coupling, $\Gamma = 850$. The reason for the weak sensitivity is that $g(r_{ij})$ does not distinguish between intra-shell neighbours and neighbours on different shells. This leads to a smeared out structure of $g(r_{ij})$.

The loss of order is reflected more clearly in the C2P correlation function. As for the 2D case, it allows to quantitatively assess the melting transition(s) for these 3D

---

[14] This cluster is formed from 4.86 μm particles at a gas pressure of 6.4 Pa and at a rf power of 1.3 W.

clusters. This is shown in figure 12 for the same cluster ($N = 60$) with or without laser heating. As for the 2D case, one sees pronounced peaks at distinct angles φ and radii r_{II} at low heating powers and subsequent loss of correlations for increased heating (reduced Γ). Also, in these 3D systems, laser heating provides a near-equilibrium heating scenario. A two-step melting (orientational melting before radial melting) which is expected for finite clusters [51, 52, 126, 179] is experimentally identified also for 3D clusters [97].

Finally, as another example of a liquid state property, the diffusion constant D, equation (8), has been derived from the experimental 3D particle trajectories of the $N = 60$ cluster, based on the analysis of unstable INMs [142, 171, 177], see section 2.5. The so obtained diffusion coefficient is shown in figure 13. For comparison, also the diffusion constants of clusters of different sizes are added [177]. A linear relationship between D and temperature is found for all studied clusters where D reaches values of about $D = 1.3 \times 10^{-6}\,\text{m}^2/\text{s}$ at the highest dust temperatures, $T \approx 4 \times 10^4\,\text{K}$. The values for the diffusion coefficient are decisively larger than in the 2D case [142, 171]. A reason for this is the higher dimensionality of the system that allows more paths to change configurations[15].

As discussed in section 5.2, from the diffusion constant an approximate melting temperature can be extrapolated which is then found to be $T_{\text{M}} \approx 2010\,\text{K}$ for $N = 60$. Interestingly, this is smaller than the kinetic temperature of this cluster even in the absence of heating which is $T_{\text{kin}} = 2930\,\text{K}$ [177]. This relatively high kinetic temperature, even in the unheated case, is explained by additional heating processes by the wake-field instability caused by streaming ions in the plasma sheath [180–182].

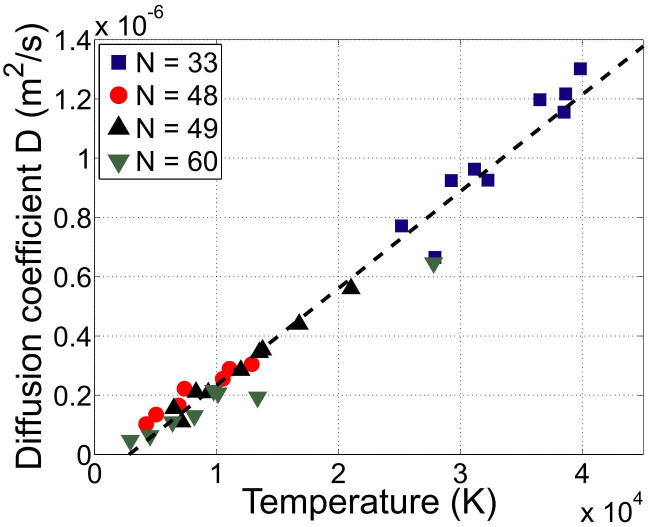

Figure 13. Diffusion coefficient $D(T)$ as a function of temperature for Yukawa balls of different size determined from an INM analysis. The dashed line corresponds to a linear fit to the diffusion coefficients for all clusters. Reproduced with permission from [177], Copyright 2013 American Physical Society.

7. Discussion and outlook

7.1. Discussion of the results

In this review, we discussed the various opportunities provided by laser beams as manipulation tools for dusty plasmas. We focused on the use of lasers as heating instruments for dust particles. As discussed in the introduction, various further uses, like the excitation of shear stress [88, 89] or of the rotation of a cluster shell [53], are possible as well, but this goes beyond the scope of this review. The availability of reliable heating tools is essential for the experimental investigation of phase transitions and instabilities in dust crystals. The enhanced manipulation setup for finite 2D dust clusters, presented in section 3.1, has proven to be usable as a tunable thermostat in both experiment and LMD simulation. The experiments confirmed that the used laser heating scheme provides a homogeneous power input over the entire cluster and over all frequencies. As desirable for a true thermal heating, the isotropy and the Maxwellian shape of the velocity distribution are preserved to very high accuracy. Various laser scanning concepts have been studied in the simulations allowing to predict the optimal parameters for the experiments.

The laser heating method was used to perform temperature scans of small 2D dust clusters with different particle numbers. The INM analysis allowed us to calculate the diffusion constant and, by this, to determine an approximate melting temperature. This melting temperature is found to be crucially dependent on the exact particle number, as a consequence of different cluster symmetries. At the same time the INM analysis does not allow to discriminate between intra-shell and inter-shell melting. As another more sensitive quantity we studied the C2P correlation function which displays both intra-shell and inter-shell correlation.

The heating method for 3D dust clusters has to work with two opposing laser beams, due to the required space for diagnostics and illumination of the cluster. Hence, the heating quality with respect to the isotropy and the Maxwellian shape of the velocity distribution is not as perfect as for 2D clusters. Nevertheless, as in 2D, the quality of this heating technique is sufficient to manipulate the dust temperature (and hence the coupling strength) in a controlled manner, without affecting the plasma parameters. Due to the spherical symmetry of 3D Yukawa balls, structural parameters which take into account this symmetry are required in order to investigate the structure and the melting behaviour of these systems. The most sensitive quantity turned out to be the C2P correlation function which displays both intra-shell and inter-shell correlation and allows us to distinguish solid clusters with a highly ordered structure from molten clusters. While important aspects of the melting behaviour in 3D are now understood, accurate data for the phase diagram and its the particle number dependence are still missing. The presented experimental tool–laser heating–, combined with the diagnostic based on the C2P correlation function should allow to study these questions in detail in the near future.

---

[15] From the relation of the diffusion coefficient to the mean squared displacements, equation (5), one would expect a dimensionality-related increase by a factor 3/2 which, however, is not suffcient to explain the observed difference of the experimental values. This problem is still under investigation.

7.2. Extension to transport properties of inhomogeneous strongly coupled systems

Both experiments and LMD simulations have shown that an appropriate heating scheme allows for a homogeneous heating of the entire 2D cluster [96, 157]. However, this heating method can also be used to heat only a selected spatial region. As long as the heated region is larger than the laser spot size, local heating is simply realized by restricting the area which is scanned by the laser spots. Kudelis *et al* suggested an experiment where only the central region of a 2D Yukawa cluster is heated by four randomly moving laser spots and performed LMD simulations for this scenario [158]. The thermal conductivity associated with the radial temperature profile, see figure 14 (bottom), is found to be constant over a wide range in coupling strengths, including the phase transition between solid and liquid [158]. This result is in good agreement with experimental data for the heat transport in an extended 2D dust crystal by Nosenko *et al* [94]. The upper part of figure 14 shows the spatial particle density of the Yukawa cluster that is heated in the inner region. While a pronounced shell structure is found at the cold outer region, the centre of the cluster is molten.

It remains an interesting task to verify these predictions in an experiment and, thus, employ laser heating for the measurement of heat transport in strongly correlated finite dusty plasmas. Another interesting task is to study the influence of an electric or magnetic field on the transport coefficients.

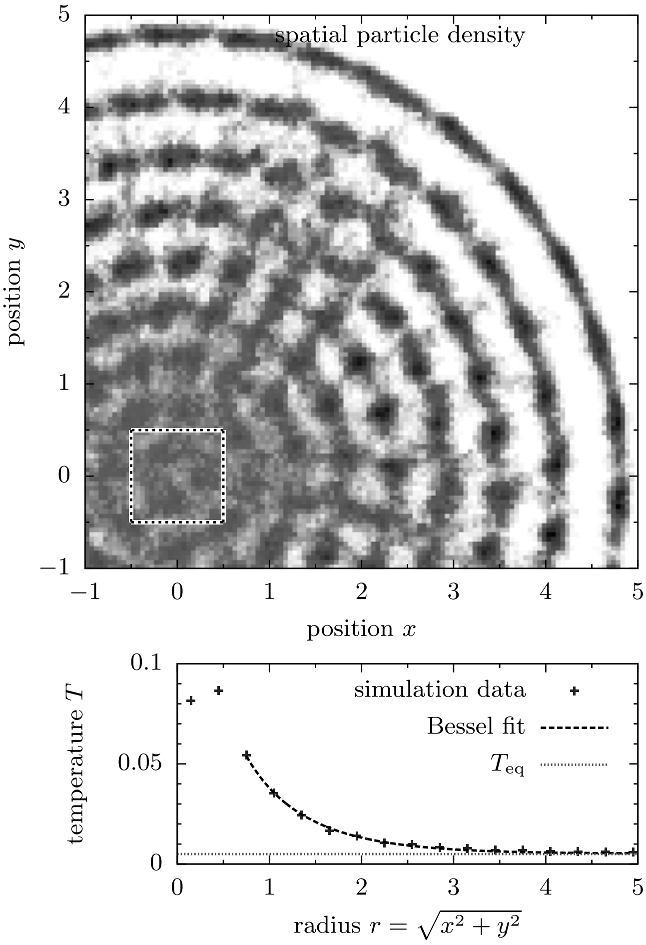

Figure 14. Top: spatial density of a Yukawa cluster with $N = 200$ particles. Four randomly moving laser spots heat the inner square marked by the dashed rectangle. Bottom: radial temperature profile and the fit by the analytical model presented in [158]. The temperature towards the border approaches the equilibrium temperature T_{eq} of the unheated cluster.

7.3. Control of time-dependent processes in complex plasmas

The applications discussed so far all considered stationary states. However, the laser heating method also allows for the study of transient, time-dependent processes. Compared to the relatively slow time scale of the heavy dust particles, the power input can be turned on and off practically immediately by switching on an off the external laser source. A possible application is a temperature quench during which the system is abruptly cooled (or heated). This allows, for example, to study the time-dependent relaxation from a fluid into a crystalline state. Alternatively, quenching of a dust crystal was achieved by changing the properties of the ambient plasma, e.g. via a sinusoidal modulation of the dc self-bias of the lower, powered electrode [183], or by applying shock waves induced via a wire placed beneath the crystal [184, 185]. However, this alters the plasma environment and does not allow to vary only Γ by a single parameter, namely the dust kinetic temperature, like in the laser experiments presented in this review.

Feng *et al* [166] laser-heated, and subsequently rapidly cooled, a 2D dust crystal that initially was arranged in a hexagonal lattice. During rapid heating, the dust arrangement remained in a solid structure at temperatures above the melting point, demonstrating solid superheating. The relaxation of small, 2D dust clusters was investigated by means of lasers by Lisin *et al* [186]. There and in [184], the cooling rate for the crystallization of a 2D dust system was found to be close to the friction coefficient, at moderate damping rates. A different behaviour was found in laser-mediated recrystallization experiments with small 3D dust clouds [187] where the cooling rate was found to be decisively lower than the friction coefficient for moderate damping (i.e. $\omega_0 \approx \gamma$), confirming previous simulations [188]. However, further investigations are required to study the shell formation process in larger dust clouds with several thousand particles and a multi-shell structure. A possible approach to circumvent the obstacle of high particle numbers could be the use of tracer particles to artificially reduce the particle density [189, 190].

Furthermore, since dust clusters are, at low neutral gas pressure, strongly influenced by wake effects due to fast streaming ions and thus exhibit attractive forces leading to particle chain formation [63, 64], it would be tempting to apply a laser-induced torque to the dust system in order to study the energetic landscape by screwing the aligned dust ensemble.

A particularly interesting application would be a temperature quench in the presence of a strong magnetic field. Ott *et al* found in MD simulations that a magnetic field may prevent crystallization. This is unexpected since, due to the Bohr von Leeuwen theorem, a magnetic field should not affect the static properties of a classical system. The reason for the observed effect is that a strong magnetic field may prevent conversion of potential energy into kinetic energy creating a bottleneck for a phase transition. Above a critical magnetic field strength, the relaxation time τ_r for the crystallization increases exponentially [191]. It would be very interesting to verify these simulation results in a laser heating experiment. So far magnetizing dust particles in an experiment has not been possible which is due to the low specific charge Q_d/m of the dust grains. An alternative way to effectively 'magnetize' the dust component is to put the cluster into rotation via a rotation of the neutral gas [192]. The Coriolis force then has the same functional form, $\vec{F}_C \propto \vec{v} \times \vec{\omega}$, as the Lorentz force and acts as a 'pseudo-magnetic' field (Larmor's theorem). This idea has in fact been realized in dusty plasma experiments. It was shown that important properties such as collective modes of magnetized strongly correlated plasmas can be accurately reproduced [193–195]. In combination with the laser heating (or cooling) method presented in this paper, this technique should allow to perform temperature quenches in experiments with finite dust clusters and to investigate the influence of the magnetization on the relaxation time for crystallization.

This outlines just a few possible further directions of laser heating of strongly correlated finite dust clusters. Besides thermodynamic properties which were in the focus of this article, an experimental analysis of time dependent processes is now within reach. The relevance of correlation effects in many fields of physics should make such studies interesting also beyond the field of dusty plasmas.

Acknowledgments

We acknowledge financial support by the Deutsche Forschungsgemeinschaft via SFB-TR 24, grants A3, A7 and A9 and a grant for CPU time at the HLRN (grant SHP006), the HEPP and M Mulsow for the help with data processing.

References

[1] Ivlev A, Löwen H, Morfill G and Royall C P 2012 *Complex Plasmas and Colloidal Dispersions: Particle-Resolved Studies of Classical Liquids and Solids (Series in Soft Condensed Matter)* (Singapore: World Scientific)
[2] Meichsner J, Bonitz M, Piel A and Feske H 2012 *Contrib. Plasma Phys.* **52** 789
[3] Bonitz M, Horing N and Ludwig P (ed) 2010 *Introduction to Complex Plasmas* (Berlin: Springer)
[4] Bonitz M, Becker K, Lopez J and Thomsen H (ed) 2014 *Complex Plasmas: Scientific Challenges and Technological Opportunities* 1st edn (Berlin: Springer)
[5] Melzer A, Trottenberg T and Piel A 1994 *Phys. Lett.* A **191** 301–8
[6] Bonitz M, Henning C and Block D 2010 *Rep. Prog. Phys.* **73** 066501
[7] Ott T, Stanley M and Bonitz M 2011 *Phys. Plasmas* **18** 063701
[8] Ichimaru S 1982 *Rev. Mod. Phys.* **54** 1017–59
[9] Hartmann P, Kalman G J, Donkó Z and Kutasi K 2005 *Phys. Rev.* E **72** 026409
[10] Bonitz M *et al* 2008 *Phys. Plasmas* **15** 055704
[11] Chu J H and I L 1994 *Phys. Rev. Lett.* **72** 4009–12
[12] Thomas H, Morfill G E, Demmel V, Goree J, Feuerbacher B and Möhlmann D 1994 *Phys. Rev. Lett.* **73** 652–5
[13] Hayashi Y and Tachibana K 1994 *Japan. J. Appl. Phys.* **33** L804
[14] Morfill G E, Thomas H M, Konopka U, Rothermel H, Zuzic M, Ivlev A and Goree J 1999 *Phys. Rev. Lett.* **83** 1598–601
[15] Rothermel H, Hagl T, Morfill G E, Thoma M H and Thomas H M 2002 *Phys. Rev. Lett.* **89** 175001
[16] Schmidt C, Arp O and Piel A 2011 *Phys. Plasmas* **18** 013704
[17] Melzer A, Homann A and Piel A 1996 *Phys. Rev.* E **53** 2757–66
[18] Thomas H M and Morfill G E 1996 *Nature* **379** 806–9
[19] Ivlev A V, Konopka U, Morfill G and Joyce G 2003 *Phys. Rev.* E **68** 026405
[20] Couëdel L, Mikikian M, Samarian A A and Boufendi L 2010 *Phys. Plasmas* **17** 083705
[21] Ivanov Y and Melzer A 2005 *Phys. Plasmas* **12** 072110
[22] Land V and Goedheer W 2007 *IEEE Trans. Plasma Sci.* **35** 280–5
[23] Rosenberg M and Mendis D A 1995 *IEEE Trans. Plasma Sci.* **23** 177–9
[24] Rosenberg M, Mendis D A and Sheehan D P 1996 *IEEE Trans. Plasma Sci.* **24** 1422–30
[25] Samarian A A, Vaulina O S, Nefedov A P, Fortov V E, James B W and Petrov O F 2001 *Phys. Rev.* E **64** 056407
[26] Samarian A A and Vaulina O S 2000 *Phys. Lett.* A **278** 146–51
[27] Bloch I 2005 *J. Phys. B: At. Mol. Opt. Phys.* **38** S629
[28] Mikhael J, Gera G, Bohlein T and Bechinger C 2011 *Soft Matter* **7** 1352–7
[29] Bohlein T and Bechinger C 2012 *Phys. Rev. Lett.* **109** 058301
[30] Tajima T and Dawson J 1979 *Phys. Rev. Lett.* **43** 267
[31] Joshi C, Mori W B, Katsouleas T, Dawson J M, Kindel J M and Forslund D W 1984 *Nature* **311** 525–9
[32] Pukhov A and Meyer-ter Vehn J 2002 *Appl. Phys.* B **74** 355
[33] Katsouleas T 2006 *Nature* **431** 515
[34] Geddes C, Toth C, van Tilborg J, Esarey E, Schroder C, Bruhwiler D, Nieter C, Cary J and Leemans W 2004 *Nature* **431** 538
[35] Hegelich B, Albright B, Cobble J, Flippo K, Letzring S, Paffett M, Ruhl H, Schreiber S, Schulze R and Fernandez J 2006 *Nature* **439** 441
[36] Lu W, Tzoufras M, Joshi C, Tsung F S, Mori W B, Vieira J, Fonseca R A and Silva L O 2007 *Phys. Rev. Spec. Top. Accel. Beams* **10** 061301
[37] Ashkin A, Dziedzic J M, Bjorkholm J E and Chu S 1986 *Opt. Lett.* **11** 288–90
[38] Ashkin A 1997 *Methods in Cell Biology* vol 55, ed P Michael Sheetz (San Diego: Academic) pp 1–27
[39] Ashkin A 2000 *IEEE J. Sel. Top. Quantum Electron.* **6** 841–56
[40] Grier D G 2003 *Nature* **424** 810–6
[41] Rousse A *et al* 2001 *Nature* **410** 65–8
[42] Sokolowski-Tinten K *et al* 2003 *Nature* **422** 287
[43] Kremp D, Bornath T, Bonitz M and Schlanges M 1999 *Phys. Rev.* E **60** 4725–32
[44] Bonitz M, Bornath T, Kremp D, Schlanges M and Kraeft W D 1999 *Contrib. Plasma Phys.* **39** 329
[45] Haberland H, Bonitz M and Kremp D 2001 *Phys. Rev.* E **64** 026405
[46] Theobald W, Hässner R, Wülker C and Sauerbrey R 1996 *Phys. Rev. Lett.* **77** 298
[47] Roth M *et al* 2001 *Phys. Rev. Lett.* **86** 436–9
[48] Tabak M, Hammer J, Glinsky M, Kruer W, Wilks S, Woodworth J, Campbell E and Perry M 1994 *Phys. Plasmas* **1** 1626
[49] Juan W, Huang Z, Hsu J, Lai Y and I L 1998 *Phys. Rev.* E **58** R6947
[50] Lai Y J and I L 1999 *Phys. Rev.* E **60** 4743–53
[51] Bedanov V M and Peeters F 1994 *Phys. Rev.* B **49** 2667
[52] Schweigert V A and Peeters F 1995 *Phys. Rev.* B **51** 7700

[53] Klindworth M, Melzer A, Piel A and Schweigert V A 2000 *Phys. Rev.* B **61** 8404

[54] Melzer A 2003 *Phys. Rev.* E **67** 016411

[55] Arp O, Block D, Piel A and Melzer A 2004 *Phys. Rev. Lett.* **93** 165004

[56] Henning C, Fujioka K, Ludwig P, Piel A, Melzer A and Bonitz M 2008 *Phys. Rev. Lett.* **101** 045002

[57] Olivetti A, Barre J, Marcos B, Bouchet F and Kaiser R 2009 *Phys. Rev. Lett.* **103** 224301

[58] Bauch S, Balzer K, Henning C and Bonitz M 2009 *Phys. Rev.* B **80** 054515

[59] Kählert H, Kalman G and Bonitz M 2014 *Phys. Rev.* E **90** 011101(R)

[60] Abraham J W, Bonitz M, McDonald C, Orlando G and Brabec T 2014 *New J. Phys.* **16** 013001

[61] McDonald C R, Orlando G, Abraham J W, Hochstuhl D, Bonitz M and Brabec T 2013 *Phys. Rev. Lett.* **111** 256801

[62] Abraham J W and Bonitz M 2014 *Contrib. Plasma Phys.* **54** 27–99

[63] Kroll M, Schablinski J, Block D and Piel A 2010 *Phys. Plasmas* **17** 013702

[64] Ludwig P, Miloch W, Kählert H and Bonitz M 2012 *New J. Phys.* **14** 053016

[65] Block D, Carstensen J, Ludwig P, Miloch W, Greiner F, Piel A, Bonitz M and Melzer A 2012 *Contrib. Plasma Phys.* **52** 804

[66] Meiwes-Broer K H (ed) 2000 *Metal Clusters at Surfaces: Structure, Quantum Properties, Physical Chemistry* (Berlin: Springer)

[67] Haberland H, Hippler T, Donges J, Kostko O, Schmidt M and von Issendorff B 2005 *Phys. Rev. Lett.* **94** 035701

[68] Buffat P and Borel J P 1976 *Phys. Rev.* A **13** 2287–98

[69] Lai S L, Carlsson J R A and Allen L H 1998 *Appl. Phys. Lett.* **72** 1098–100

[70] Dippel M, Maier A, Gimple V, Wider H, Evenson W E, Rasera R L and Schatz G 2001 *Phys. Rev. Lett.* **87** 095505

[71] Reiss H, Mirabel P and Whetten R L 1988 *J. Phys. Chem.* **92** 7241–6

[72] Vaneet R R and Mochel J 1995 *Surf. Sci.* **341** 40–50

[73] Qi Y, Çağin T, Johnson W L and Goddard W A 2001 *J. Chem. Phys.* **115** 385–94

[74] Ding F, Rosén A and Bolton K 2004 *Phys. Rev.* B **70** 075416

[75] Schiffer J P 2002 *Phys. Rev. Lett.* **88** 205003

[76] Ditmire T, Smith R A, Tisch J W G and Hutchinson M H R 1997 *Phys. Rev. Lett.* **78** 3121–4

[77] Köller L, Schumacher M, Köhn J, Teuber S, Tiggesbäumker J and Meiwes-Broer K H 1999 *Phys. Rev. Lett.* **82** 3783–6

[78] Antonsen T M, Taguchi T, Gupta A, Palastro J and Milchberg H M 2005 *Phys. Plasmas* **12** 056703

[79] Milchberg H M, McNaught S J and Parra E 2001 *Phys. Rev.* E **64** 056402

[80] Fennel T, Meiwes-Broer K H, Tiggesbäumker J, Reinhard P G, Dinh P M and Suraud E 2010 *Rev. Mod. Phys.* **82** 1793–842

[81] Dufty J and Bonitz M 2005 *J. Phys. Conf. Ser.* **11** 47–60

[82] Fromm A, Bonitz M and Dufty J 2008 *Ann. Phys.* **323** 3158–74

[83] Saalmann U, Siedschlag C and Rost J M 2006 *J. Phys. B: At. Mol. Opt. Phys.* **39** R39

[84] Krainov V and Smirnov M 2002 *Phys. Rep.* **370** 237–331

[85] Shim B, Hays G, Zgadzaj R, Ditmire T and Downer M C 2007 *Phys. Rev. Lett.* **98** 123902

[86] Erk B, Hoffmann K, Kandadai N, Helal A, Keto J and Ditmire T 2011 *Phys. Rev.* A **83** 043201

[87] Piel A and Goree J 2013 *Phys. Rev.* E **88** 063103

[88] Nosenko V and Goree J 2004 *Phys. Rev. Lett.* **93** 155004

[89] Feng Y, Goree J and Liu B 2012 *Phys. Rev. Lett.* **109** 185002

[90] Melzer A, Nunomura S, Samsonov D, Ma Z W and Goree J 2000 *Phys. Rev.* E **62** 4162–76

[91] Nosenko V, Goree J, Ma Z W and Piel A 2002 *Phys. Rev. Lett.* **88** 135001

[92] Wolter M and Melzer A 2005 *Phys. Rev.* E **71** 036414

[93] Nosenko V, Goree J and Piel A 2006 *Phys. Plasmas* **13** 032106

[94] Nosenko V, Zhdanov S, Ivlev A V, Morfill G, Goree J and Piel A 2008 *Phys. Rev. Lett.* **100** 025003

[95] Goree J, Liu B and Feng Y 2013 *Plasma Phys. Control. Fusion* **55** 124004

[96] Schablinski J, Block D, Piel A, Melzer A, Thomsen H, Kählert H and Bonitz M 2012 *Phys. Plasmas* **19** 013705

[97] Schella A, Miksch T, Melzer A, Schablinski J, Block D, Piel A, Thomsen H, Ludwig P and Bonitz M 2011 *Phys. Rev.* E **84** 056402

[98] Strandburg K J 1988 *Rev. Mod. Phys.* **60** 161–207

[99] Chui S T 1983 *Phys. Rev. B* **28** 178–94

[100] Kosterlitz J M and Thouless D J 1973 *J. Phys. C: Solid State Phys.* **6** 1181

[101] Nelson D R and Halperin B I 1979 *Phys. Rev.* B **19** 2457–84

[102] Young A P 1979 *Phys. Rev.* B **19** 1855–66

[103] Derzsi A, Kovács A Z, Donkó Z and Hartmann P 2014 *Phys. Plasmas* **21** 023706

[104] Apolinario S W S and Peeters F M 2007 *Phys. Rev.* E **76** 031107

[105] Kong M, Partoens B and Peeters F M 2003 *Phys. Rev.* E **67** 021608

[106] Arp O, Block D, Klindworth M and Piel A 2005 *Phys. Plasmas* **12** 122102

[107] Block D, Kroll M, Arp O, Piel A, Käding S, Ivanov Y, Melzer A, Henning C, Baumgartner H, Ludwig P and Bonitz M 2007 *Plasma Phys. Control. Fusion* **49** B109

[108] Hasse R W and Avilov V V 1991 *Phys. Rev.* A **44** 4506–15

[109] Schiffer J P 1988 *Phys. Rev. Lett.* **61** 1843–6

[110] Ludwig P, Kosse S and Bonitz M 2005 *Phys. Rev.* E **71** 046403

[111] Bonitz M, Block D, Arp O, Golubnychiy V, Baumgartner H, Ludwig P, Piel A and Filinov A 2006 *Phys. Rev. Lett.* **96** 075001

[112] Baumgartner H, Asmus D, Golubnychiy V, Ludwig P, Kählert H and Bonitz M 2008 *New J. Phys.* **10** 093019

[113] Henning C, Baumgartner H, Piel A, Ludwig P, Golubnichiy V, Bonitz M and Block D 2006 *Phys. Rev.* E **74** 056403

[114] Henning C, Ludwig P, Filinov A, Piel A and Bonitz M 2007 *Phys. Rev.* E **76** 036404

[115] Wrighton J, Dufty J W, Kählert H and Bonitz M 2009 *Phys. Rev.* E **80** 066405

[116] Wrighton J, Dufty J, Bonitz M and Kählert H 2010 *Contrib. Plasma Phys.* **50** 26–30

[117] Bruhn H, Kählert H, Ott T, Bonitz M, Wrighton J and Dufty J W 2011 *Phys. Rev.* E **84** 046407

[118] Wrighton J, Kählert H, Ott T, Ludwig P, Thomsen H, Dufty J and Bonitz M 2012 *Contrib. Plasma Phys.* **52** 45–8

[119] Käding S and Melzer A 2006 *Phys. Plasmas* **13** 090701

[120] Käding S, Block D, Melzer A, Piel A, Kählert H, Ludwig P and Bonitz M 2008 *Phys. Plasmas* **15** 073710

[121] Kählert H, Ludwig P, Baumgartner H, Bonitz M, Block D, Käding S, Melzer A and Piel A 2008 *Phys. Rev.* E **78** 036408

[122] Baumgartner H, Block D and Bonitz M 2009 *Contrib. Plasma Phys.* **49** 281–302

[123] Golubnichiy V, Baumgartner H, Bonitz M, Filinov A and Fehske H 2006 *J. Phys. A: Math. Gen.* **39** 4527

[124] Filinov A V, Lozovik Y E and Bonitz M 2000 *Phys. Status Solidi* b **221** 231

[125] Filinov A V, Bonitz M and Lozovik Y E 2001 *Phys. Rev. Lett.* **86** 3851

[126] Apolinario S, Partoens B and Peters F 2007 *New J. Phys.* **9** 283

[127] Ludwig P, Thomsen H, Balzer K, Filinov A and Bonitz M 2010 *Plasma Phys. Control. Fusion* **52** 124013
[128] Daligault J 2006 *Phys. Rev. Lett.* **96** 065003
[129] Ott T and Bonitz M 2011 *Phys. Rev. Lett.* **107** 135003
[130] Juan W T and I L 1998 *Phys. Rev. Lett.* **80** 3073–6
[131] Hou L J, Piel A and Shukla P K 2009 *Phys. Rev. Lett.* **102** 085002
[132] Ott T, Bonitz M and Hartmann P 2009 *Phys. Rev. Lett.* **103** 099501
[133] Ott T and Bonitz M 2009 *Contrib. Plasma Phys.* **49** 760
[134] Ott T and Bonitz M 2009 *Phys. Rev. Lett.* **103** 195001
[135] Ott T, Löwen H and Bonitz M 2014 *Phys. Rev.* E **89** 013105
[136] Vaulina O S, Adamovich X G, Petrov O F and Fortov V E 2008 *Phys. Rev.* E **77** 066404
[137] Seeley G and Keyes T 1989 *J. Chem. Phys.* **91** 5581–6
[138] Stratt R M 1995 *Acc. Chem. Res.* **28** 201–7
[139] Keyes T 1997 *J. Phys. Chem. A* **101** 2921–30
[140] Vijayadamodar G V and Nitzan A 1995 *J. Chem. Phys.* **103** 2169–77
[141] Keyes T, Vijayadamodar G V and Zurcher U 1997 *J. Chem. Phys.* **106** 4651–7
[142] Melzer A, Schella A, Schablinski J, Block D and Piel A 2013 *Phys. Rev.* E **87** 033107
[143] Donkó Z, Kalman G J and Golden K I 2002 *Phys. Rev. Lett.* **88** 225001
[144] Das S P 2004 *Rev. Mod. Phys.* **76** 785–851
[145] Maurer H R and Kersten H 2011 *J. Phys. D: Appl. Phys.* **44** 174029
[146] Fisher R, Avinash K, Thomas E, Merlino R and Gupta V 2013 *Phys. Rev.* E **88** 031101
[147] Homann A, Melzer A, Peters S, Madani R and Piel A 1997 *Phys. Rev.* E **56** 7138–41
[148] Annaratone B 1997 *Int. Conf. on Phenomena in Ionized Gases* vol 07 C4 pp 155–65
[149] Takahashi K, Oishi T, Shimomai K, Hayashi Y and Nishino S 1998 *Phys. Rev.* E **58** 7805–11
[150] Piel A and Melzer A 2002 *Plasma Phys. Control. Fusion* **44** R1–26
[151] Homann A, Melzer A, Peters S, Madani R and Piel A 1998 *Phys. Lett.* A **242** 173–80
[152] Homann A, Melzer A and Piel A 1999 *Phys. Rev.* E **59** R3835
[153] Melzer A, Schweigert V A and Piel A 2000 *Phys. Scr.* **61** 494–501
[154] Samarian A A and Vladimirov S V 2009 *Contrib. Plasma Phys.* **49** 260–80
[155] Nosenko V, Goree J, Ma Z W, Dubin D H E and Piel A 2003 *Phys. Rev.* E **68** 056409
[156] Piel A, Nosenko V and Goree J 2006 *Phys. Plasmas* **13** 042104
[157] Thomsen H, Kählert H, Bonitz M, Schablinski J, Block D, Piel A and Melzer A 2012 *Phys. Plasmas* **19** 023701
[158] Kudelis G, Thomsen H and Bonitz M 2013 *Phys. Plasmas* **20** 073701
[159] Liu B, Goree J, Nosenko V and Boufendi L 2003 *Phys. Plasmas* **10** 9–20
[160] Thomsen H 2011 Excitation and melting of Yukawa balls *Diploma Thesis* Institut für Theoretische Physik und Astrophysik der Christian-Albrechts-Universität zu Kiel
[161] Mannella R 2004 *Phys. Rev.* E **69** 041107
[162] Spreiter Q and Walter M 1999 *J. Comput. Phys.* **152** 102–19
[163] Chin S A 2008 *Phys. Rev.* E **77** 066401
[164] Ott T, Baiko D A, Kählert H and Bonitz M 2013 *Phys. Rev.* E **87** 043102
[165] Nosenko V, Zhdanov S K, Ivlev A V, Knapek C A and Morfill G E 2009 *Phys. Rev. Lett.* **103** 015001
[166] Feng Y, Goree J and Liu B 2008 *Phys. Rev. Lett.* **100** 205007
[167] Chan C L, Woon W Y and I L 2004 *Phys. Rev. Lett.* **93** 220602
[168] Nunomura S, Samsonov D, Zhdanov S and Morfill G 2005 *Phys. Rev. Lett.* **95** 025003
[169] Liu B, Goree J and Vaulina O S 2006 *Phys. Rev. Lett.* **96** 015005
[170] Feng Y, Goree J and Liu B 2010 *Phys. Rev. Lett.* **104** 165003
[171] Melzer A, Schella A, Schablinski J, Block D and Piel A 2012 *Phys. Rev. Lett.* **108** 225001
[172] Böning J, Filinov A, Ludwig P, Baumgartner H, Bonitz M and Lozovik Y E 2008 *Phys. Rev. Lett.* **100** 113401
[173] Annaratone B M, Antonova T, Goldbeck D D, Thomas H M and Morfill G E 2004 *Plasma Phys. Control. Fusion* **46** B495
[174] Antonova T, Annaratone B M, Allen J E, Sato T, Thomas H M and Morfill G E 2009 *New J. Phys.* **11** 113023
[175] Schella A, Mulsow M, Melzer A, Kählert H, Block D, Ludwig P and Bonitz M 2013 *New J. Phys.* **15** 113021
[176] Block D, Käding S, Melzer A, Piel A, Baumgartner H and Bonitz M 2008 *Phys. Plasmas* **15** 040701
[177] Schella A, Mulsow M, Melzer A, Schablinski J and Block D 2013 *Phys. Rev.* E **87** 063102
[178] Himpel M, Buttenschön B and Melzer A 2011 *Rev. Sci. Instrum.* **82** 053706
[179] Apolinario S, Partoens B and Peters F 2008 *Phys. Rev.* B **77** 035321
[180] Schweigert V A, Schweigert I V, Melzer A, Homann A and Piel A 1996 *Phys. Rev.* E **54** 4155
[181] Schweigert V A, Schweigert I V, Melzer A, Homann A and Piel A 1998 *Phys. Rev. Lett.* **80** 5345
[182] Melandsø F 1997 *Phys. Rev.* E **55** 7495
[183] Hartmann P, Douglass A, Reyes J C, Matthews L S, Hyde T W, Kovács A and Donkó Z 2010 *Phys. Rev. Lett.* **105** 115004
[184] Knapek C A, Samsonov D, Zhdanov S, Konopka U and Morfill G E 2007 *Phys. Rev. Lett.* **98** 015004
[185] Knapek C A, Durniak C, Samsonov D and Morfill G E 2013 *Phys. Rev. Lett.* **110** 035001
[186] Lisin E A, Timirkhanov R A, Vaulina O S, Petrov O F and Fortov V E 2013 *New J. Phys.* **15** 053004
[187] Schella A, Mulsow M and Melzer A 2014 *Phys. Plasmas* **21** 050701
[188] Kählert H and Bonitz M 2010 *Phys. Rev. Lett.* **104** 015001
[189] Miksch T and Melzer A 2007 *Phys. Rev.* E **75** 016404
[190] Himpel M, Killer C, Buttenschön B and Melzer A 2012 *Phys. Plasmas* **19** 123704
[191] Ott T, Löwen H and Bonitz M 2013 *Phys. Rev. Lett.* **111** 065001
[192] Carstensen J, Greiner F and Piel A 2010 *Phys. Plasmas* **17** 083703
[193] Kählert H, Carstensen J, Bonitz M, Löwen H, Greiner F and Piel A 2012 *Phys. Rev. Lett.* **109** 155003
[194] Bonitz M, Kählert H, Ott T and Löwen H 2013 *Plasma Sources Sci. Technol.* **22** 015007
[195] Hartmann P, Donkó Z, Ott T, Kählert H and Bonitz M 2013 *Phys. Rev. Lett.* **111** 155002